

Under-ice acoustic navigation using real-time model-aided range estimation

EeShan C. Bhatt,^{1, 2, a} Oscar Viquez,² and Henrik Schmidt²

¹*MIT-WHOI Joint Program in Oceanography/Applied Ocean Science & Engineering,
Cambridge and Woods Hole, MA, USA*

²*Department of Mechanical Engineering, Massachusetts Institute of Technology,
Cambridge, MA*

(Dated: 21 February 2022)

1 The long baseline (LBL) underwater navigation paradigm relies on the conversion
2 of recorded travel times into pseudoranges to trilaterate position. For real-time op-
3 erations, this conversion has assumed an isovelocity sound speed. For re-navigation
4 in post-processing, computationally and/or labor intensive acoustic modeling may
5 be employed to reduce uncertainty driven by multipath arrivals. This work demon-
6 strates a real-time ray-based prediction method of the effective sound speed along
7 a path from source to receiver to minimize vehicle position error. This method was
8 implemented for a small scale AUV-LBL system in March 2020, in the Beaufort Sea,
9 in total ice-covered conditions and a double ducted acoustic propagation environ-
10 ment. The vehicle was successfully deployed and recovered. Given the lack of GPS
11 data throughout the vehicle’s mission, however, the pseudorange performance is first
12 evaluated on connections between GPS-linked beacons. The real-time ranging error
13 between beacons is roughly 11 meters at distances up to 3 km. But a consistent over-
14 estimation in the real-time method provides insights for improved eigenray filtering
15 by the number of surface bounces. An operationally equivalent pipeline is used to
16 re-position the LBL beacons and re-navigate the AUV, using a modeled, historical,
17 and a locally observed sound speed profile. The median re-navigation error is 1.84 ± 2.19 RMS m. The improved trilateration performance for suggests that this ap-
18 proach effectively extends the single meter accuracy of the deployed GNSS units into
19 the water column.

^aebhatt@whoi.edu

²¹ **I. INTRODUCTION**

²² Autonomous underwater vehicles (AUVs) are increasingly capable platforms to explore
²³ and sample the ocean, particularly for remote and/or dangerous regions. However, navi-
²⁴ gation uncertainty is a major challenge in considering AUVs as standard tools for oceano-
²⁵ graphic research. While land and air-based robots utilize information from Global Nav-
²⁶ igation Satellite Systems (GNSS) to achieve single-meter location accuracy and precision
²⁷ throughout the duration of their missions, AUVs cannot access GNSS fixes while under-
²⁸ water. Therefore, underwater vehicles have relied on any combination of dead reckoning,
²⁹ hydrodynamic models, inertial navigation systems, doppler velocity logs, and acoustic base-
³⁰ line positioning systems for navigation ([Paull *et al.*, 2014](#)). Limiting navigation error and
³¹ drift requires an AUV to periodically stall on the surface and obtain a GNSS fix to reset its
³² position error. This foolproof method of self-positioning is undesirable for stealth, adverse
³³ weather conditions, and mission efficiency, and inaccessible in a GNSS-denied situation like
³⁴ an ice-covered environment.

³⁵ Of underwater acoustic navigation systems, long baseline (LBL) is the most GPS-like
³⁶ in style and scale, and most appropriate for mitigating drift without overburdening com-
³⁷ putation or payload size on the vehicle ([Van Uffelen, 2021](#)). The state-of-the-art for LBL
³⁸ outsources depth to a pressure sensor and solves the two-dimensional localization problem
³⁹ with an isovelocity, linear scaling between one way travel time (OWTT) and range ([Eustice](#)
⁴⁰ *et al.*, 2006, 2007; [Webster *et al.*, 2009, 2012](#)). This assumption is valid for short scale op-
⁴¹ erations but oversimplifies propagation at larger scales or complex sound speed structure.

42 To achieve single meter, GNSS-like performance in a GNSS-denied environment, we demon-
 43 strate an embedded ray-based data processing algorithm to convert recorded OWTTs into
 44 pseudorange estimates. This methodology was integrated onto the AUV *Macrura*, deployed
 45 and recovered in the Beaufort Sea, in March 2020, during the Ice Exercise 2020 (ICEX20).
 46 A physics-driven methodology that received an *in situ* sound speed profile (SSP) was nec-
 47 essary despite the small operational domain because of the relatively high-risk mission en-
 48 vironment—total under-ice conditions and a variable double ducted acoustic environment.
 49 For consistency, we delineate specific definitions for timing, positioning, and navigation
 50 from [Howe et al. \(2019\)](#).

- 51 1. Timing is the ability to acquire and maintain accurate and precise time anywhere in
 52 the domain of interest within user-defined timeliness parameters
- 53 2. Positioning is the ability to accurately and precisely determine one's location refer-
 54 enced to a standard geodetic system
- 55 3. Navigation is the ability to determine current and desired position (relative or absolute)
 56 and apply corrections to course, orientation, and speed to attain a desired position
 57 anywhere in the domain of concern

58 Thus, navigation is inherently in real-time and depends on positioning; positioning depends
 59 on timing. We also suggest re-navigation and re-positioning as post-processed corollaries,
 60 which may include knowledge or processing capabilities not available *in situ*.

61 While RAFOS floats championed one way ranging for re-positioning ([Duda et al., 2006](#);
 62 [Rossby et al., 1986](#)), the ability to do so for navigation was facilitated by the advent of

63 the WHOI Micro-Modem (Singh *et al.*, 2006) and synchronized clocks (Rypkema *et al.*,
64 2017). AUV navigation efforts have achieved root mean square (RMS) localization error on
65 the order of tens of meters relative to GNSS surface position over less than ten kilometers
66 in shallow (Claus *et al.*, 2018; Eustice *et al.*, 2007; Kepper *et al.*, 2017) and deep water
67 (Jakuba *et al.*, 2008; Kunz *et al.*, 2008; Webster *et al.*, 2009). However, these efforts all used
68 a nominal sound speed for travel time conversion and the vehicles were limited to shallower
69 isovelocity regimes.

70 Localization algorithms that do consider environmental or acoustic uncertainty tend to
71 focus on longer duration and larger range experiments, where spatio-temporal variability
72 cannot be ignored. These methods have also been reserved for post-processing as they
73 can be labor intensive, computationally heavy, and/or require additional information like
74 contemporaneous data. For example, gliders navigating with kinematic flight models and
75 equipped with acoustic modems were later unambiguously associated with predicted ray
76 arrivals, resulting in roughly a kilometer error and hundred meters uncertainty over basin
77 scale propagation (Van Uffelen *et al.*, 2013). A follow up study investigated how a single
78 temporally and spatially averaged SSP could mitigate position error for a four month glider
79 mission (Van Uffelen *et al.*, 2016). Wu *et al.* (2019) cross correlate three days of real acous-
80 tic records with synthetic ones generated through ocean model snapshots from HYCOM
81 (Chassagnet *et al.*, 2007). While potentially applicable for various ocean states, this is re-
82 liant on model realism and impractical for real-time operations. A “cold start” algorithm
83 that does not require prior knowledge of track, position, or sound speed information inputs
84 a four-dimensional ocean model, constrained by tomography data, into a range dependent

85 ray code to isolate the last path detected in a full multipath pattern (Mikhalevsky *et al.*,
86 2020). Then, a representative group speed is solved for alongside position in a least squares
87 fashion. This approach is able to re-position a floating hydrophone array with an error of
88 58 m and a standard deviation of 32 m based on six sources 129–450 km away but remains
89 to seen for real-time navigation.

90 The ICEX20 AUV deployment necessitated an environmentally- and physically-driven
91 relationship between recorded travel times and estimated pseudoranges due to the multipath
92 uncertainty brought upon by an increasingly observed double ducted environment in the
93 Beaufort Sea, which some refer to as the “Beaufort Lens” (Chen *et al.*, 2019; Chen and
94 Schmidt, 2020; Litvak, 2015).

95 Given that a lens introduces significant ray refraction, the Beaufort Lens is a shorthand for
96 the spatio-temporal variability of the local temperature and sound speed maxima generally
97 around 50 to 60 m in depth. A neutrally buoyant layer of warm Pacific Summer Water
98 creates a unique double ducted environment —the upper duct degrades signal coherence
99 due to intensified ice interaction and the lower duct effectively traps sound for long range
100 propagation (Poulsen and Schmidt, 2017). Modeling output (Duda *et al.*, 2021, 2019) and
101 experimental observations (Ballard *et al.*, 2020; Bhatt, 2021) suggest that, in the Beaufort
102 Sea, the duct is persistent and widespread but not necessarily continuous; it and its acoustic
103 effects can be non-existent, minimal, or drastic. Transmissions in the upper duct, between
104 the surface ice and the lens, experience minimal attenuation but degrade in signal coherence
105 with repeated reflections under the ice. In the lower duct, between the lens and its conjugate

¹⁰⁶ depth in the Atlantic water (roughly 200 m), sound above 350 Hz is trapped near losslessly
¹⁰⁷ for long range propagation (Poulsen and Schmidt, 2017).

¹⁰⁸ The Arctic, while remote, is the perfect place to demonstrate mature navigation tech-
¹⁰⁹ nologies in real GNSS-denied conditions. Thorough reviews of uncrewed vehicle operations
¹¹⁰ in polar environments can be found in Norgren *et al.* (2014) and Barker *et al.* (2020); there
¹¹¹ is no comparable work in the Arctic for a short range AUV deployment in the Beaufort
¹¹² Lens. Seminal Arctic AUV deployments (Bellingham *et al.*, 1995; Brooke, 1981; Hayes and
¹¹³ Morison, 2002; Jackson, 1983; Light and Morison, 1989) and more recent ones (Fossum
¹¹⁴ *et al.*, 2021; Jakuba *et al.*, 2008; Kukulya *et al.*, 2010; Kunz *et al.*, 2008; Plueddemann *et al.*,
¹¹⁵ 2012; Timmermans and Winsor, 2013) witnessed the classical upward refracting sound speed
¹¹⁶ profile that is amenable to an isovelocity assumption.

¹¹⁷ Of note, despite different platforms and scales, are recent glider deployments in the
¹¹⁸ Canada Basin. In 2014, in partially ice-covered conditions, a long range LBL system with
¹¹⁹ WHOI Micro-Modems at 100 m depth exploited the lower duct for long range communication
¹²⁰ with two gliders (Freitag *et al.*, 2016; Webster *et al.*, 2015). The sound speed value measured
¹²¹ at the time of reception was used to estimate pseudorange in post-processing. The beacon-
¹²² to-beacon performance was excellent, achieving contact at ranges greater than 200 km with
¹²³ a position uncertainty of 40 m. The beacon-to-glider performance, however, deteriorated
¹²⁴ due to missed contacts outside the duct, and was not described quantitatively. In 2017,
¹²⁵ gliders were deployed in a region with no ice coverage (Graupe *et al.*, 2019). Ranges were
¹²⁶ linearly scaled by a statistical description of sound speed observations taken during the
¹²⁷ experiment, 1450 ± 6.5 m/s. This resulted in an error of 550 m, which was reduced by

128 a factor between 4 and 5, depending on the dive, using a post-processing acoustic arrival
129 matching method. Both cases exploit the lower duct for high fidelity communication at long
130 ranges. Unintuitively, the smaller scale nature of our deployment during ICEX20 is not a
131 simplifying factor. For source depths typical to vehicle operations, 30 to 200 m, the Beaufort
132 Lens introduces a shadow zone that spans from 2 to 6 kilometers in range ([Schmidt and](#)
133 [Schneider, 2016](#)).

134 Compared to previous small scale navigation efforts, the approach in this paper integrates
135 real-time model-aided data processing to estimate a representative sound speed along a path
136 from source to receiver, leveraging climatology, *in situ* data, and fast acoustic modeling. The
137 paper is organized as follows. Section [II](#) details the experimental approach and conditions
138 during ICEX20. Given that there is no GNSS ground truth for the vehicle position while
139 underway, we first evaluate the real-time ranging performance of GPS-linked beacon-to-
140 beacon communication events in section [III](#). Section [IV](#) uses insights from field data to
141 introduce a new ray filtering algorithm to improve range estimation. Section [V](#) emulates the
142 real-time processing pipeline to re-position beacon-to-beacon events and re-navigate AUV
143 *Macrura*.

¹⁴⁴ **II. OVERVIEW OF THE ICEX20 EXPERIMENT**

¹⁴⁵ The results from this paper derive from data collected while deploying the AUV *Macrura*,
¹⁴⁶ a custom Bluefin-21, during the Ice Exercise 2020 (ICEX20). The experiment was conducted
¹⁴⁷ in the Beaufort Sea, from March 8th to 11th, at roughly 71.2°N. The AUV deployment was
¹⁴⁸ supported by the Integrated Communication and Navigation Network (ICNN) ([Randeni](#)
¹⁴⁹ *et al.*, 2020, 2021; [Schneider et al., 2021](#)) a specialized implementation of the LBL solution.
¹⁵⁰ The ICNN was initially developed via numerous virtual experiments to ensure robust algo-
¹⁵¹ rithms and interfaces between different hardware components. The simulation capabilities
¹⁵² are largely physics-driven with a modular system of systems approach—an environmental
¹⁵³ simulator with sub-components for the ocean, including Arctic ice drift and ocean acoustic
¹⁵⁴ propagation; a vehicle simulator with sub-components for vehicle dynamics and navigation;
¹⁵⁵ a topside hardware simulator and acoustic communications simulator, both with a software-
¹⁵⁶ only configuration and a hardware-in-the-loop version ([Schneider and Schmidt, 2018](#)). The
¹⁵⁷ virtual environment similarly emulates the interfaces between the real components to test
¹⁵⁸ the entire software pipeline.

¹⁵⁹ **A. The Integrated Communication and Navigation Network**

¹⁶⁰ The ICNN is comprised of four ice buoys in a loose rectangle, roughly 2 km away from
¹⁶¹ a central ice camp with a topside computer, as shown in Fig. 1. Each ice buoy is outfitted
¹⁶² with a Garmin GPS 18x, with a pulse-per-second rising edge aligned to 1 microsecond and
¹⁶³ a spec sheet accuracy of 3 m, 95% of the time. They are also each equipped with a WHOI

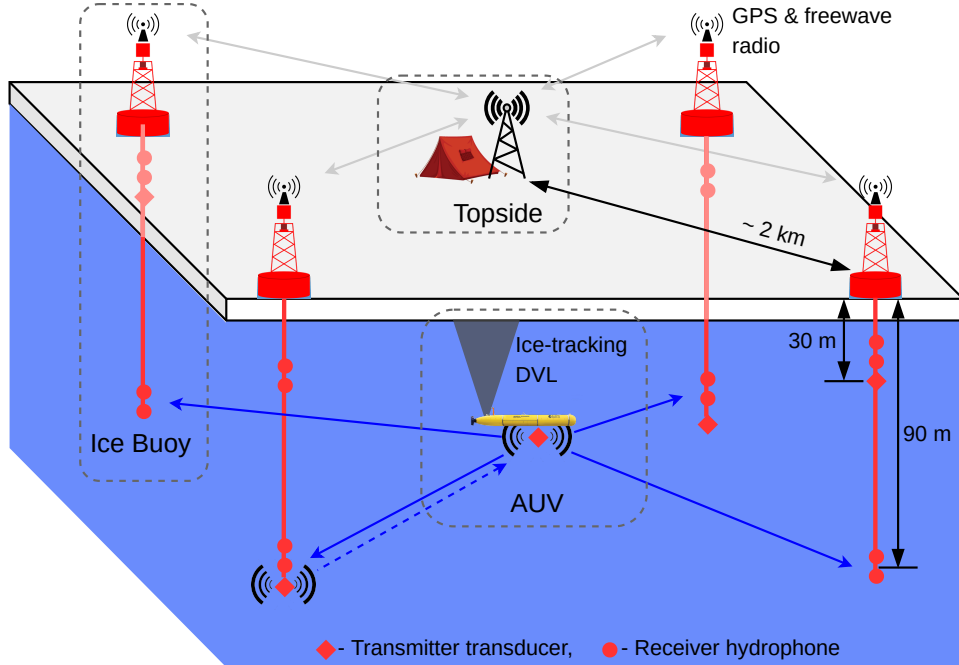


FIG. 1. A schematic overview of the Integrated Communication and Navigation Network (ICNN), which provides joint data-transfer and tracking between AUV and a human decision maker at Topside.

164 Micro-Modem ([Singh et al., 2006](#)), with a four-element receiver array, a single transmitter,
 165 and one-tenth of a millisecond resolution. Acoustic messages were sent with a 10 kHz carrier
 166 frequency, 5 kHz bandwidth, and phase-shift keying (PSK) modulation on a time-division
 167 multiple access schedule with a thirty-second cycle, giving room for two-way communication
 168 throughout the mission volume. Thus the ICNN is dependent on the successful decoding of
 169 acoustic transmissions. The receive and transmit elements were split between shallow and
 170 deeper depths—30 and 90 m—to provide better coverage across the shadow zone. While
 171 each buoy only has one transmit depth, all buoys have both receive depths but the active
 172 receive layer is consistent across all buoys. The design of the ICNN enables a self-adapting

173 network to transmit and receive at the optimal depth to maintain contact with the AUV
 174 (Schneider *et al.*, 2021). The buoys do not encompass the full horizontal range of the vehicle
 175 but are positioned to minimize overlap in trilateration for spherical positioning (Deffenbaugh
 176 *et al.*, 1996a).

177 To balance competing uses of the acoustic channel, the network uses a single synchronized
 178 digital communication packet to provide both tracking and data to the operator.

179 1. The AUV, running an ice-tracking DVL and an onboard hydrodynamic model, broad-
 180 casts its perceived location on a scheduled, time-synchronized message via WHOI
 181 Micro-Modem

182 2. Four ice buoys, each outfitted with a WHOI Micro-Modem, receive messages from the
 183 AUV and send that information over freewave radio to a Topside computer

184 3. The topside computer converts travel times into pseudorange estimates using a stochas-
 185 tic embedded prediction of the horizontal group velocity via BELLHOP ray tracing
 186 code (Porter, 2011) using a sound speed profile provided by an updatable Virtual
 187 Ocean (Bhatt *et al.*, 2022; Schneider and Schmidt, 2018)

188 4. The topside computer calculates a new position by trilaterating the range estimates
 189 5. The position differential, not the absolute position, is broadcast to the vehicle to
 190 update its navigation solution and be robust to latency and intermittency

191 In the face of GNSS-denied navigation, this approach was anecdotally successful, as shown
 192 in Fig. 2. The AUV *Macrura* was deployed through a hydrohole from an ice camp but re-
 193 covered through an emergency hydrohole. A random disk error stalled *Macrura* underneath

194 the ice but did not prevent it from transmitting its location. Due to an incoming storm, a
 195 team drilled an exploratory hole at *Macrura*'s self-reported location, and were able to drill a
 196 separate hole 1 m away to tie the vehicle off to a physical marker on the ice. Three days later,
 197 *Macrura* was recovered—the ice camp had moved over 19 km. The AUV's relative position
 198 to camp had also changed, from roughly 45°at 1000 m to 90°at 1100 m. Drama aside, we view
 199 the emergency recovery as qualitative proof of the robustness of this navigation approach.
 200 Nonetheless, this paper specifically addresses the third and fourth steps—the conversion
 201 of travel times into pseudoranges and its quantitative effect on trilateration. By focusing
 202 on pseudorange estimates between GPS-tracked beacons, and re-running the trilateration
 203 pipeline, the results are decoupled from all other mechanisms in the ICNN.

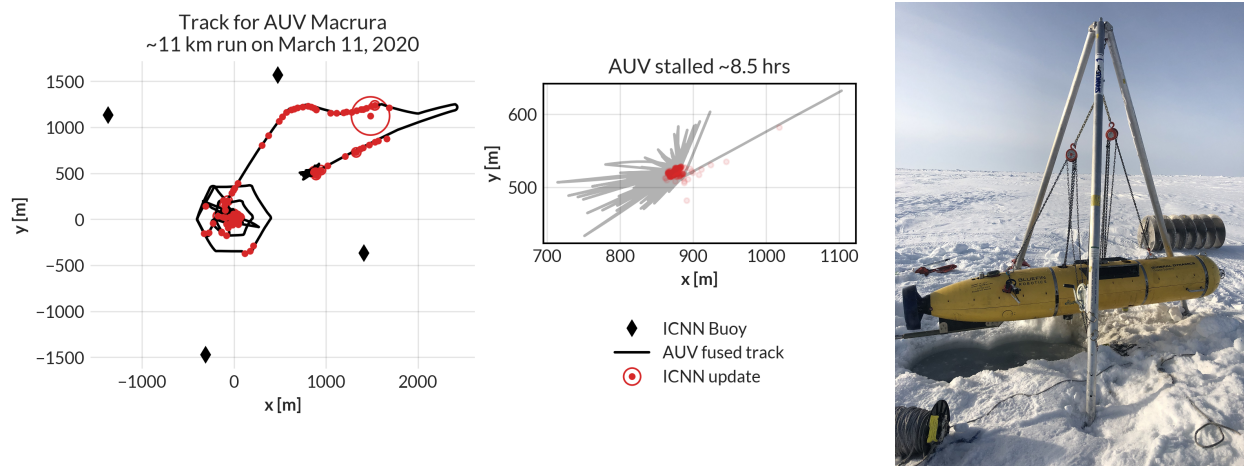


FIG. 2. The under-ice mission track for AUV *Macrura*, including the position updates as it stalled underneath the ice overnight. A marker was placed on the ice at the vehicle's estimated self-location. It was recovered after a three day storm within a meter of the marker.

204 **B. ICEX20 sound speed conditions**

205 An important component to our navigation solution is an accurate estimation of a repre-
 206 sentative SSP for the ocean volume. Previous field experience, during the Ice Exercise 2016
 207 (ICEX16), demonstrated the negative effects of the Beaufort Lens on tracking and commu-
 208 nication (Schmidt and Schneider, 2016). Fig. 3 shows historical, modeled, and *in situ* sound
 209 speed data for both ICEX16 and ICEX20. These three input streams were selected to mirror
 210 the information available on a submarine (personal conversation with LT B. Howard and LT
 211 CDR D. Goodwin). In the field, the SSP information was shared with the vehicle via basis
 212 representation compression on a lightweight digital acoustic message (Bhatt *et al.*, 2022).
 213 All modeled data comes from HYCOM (Chassagnet *et al.*, 2007), which does not seem to
 214 capture the forcing mechanisms that cause the Beaufort Lens. For ICEX16, the data-driven
 215 profile was sourced from nearby Ice Tethered Profilers (ITP) after the field experiment (Kr-
 216 ishfield *et al.*, 2008; Toole *et al.*, 2011) and exhibits a fairly deep lens; the historical profile is
 217 from the World Ocean Atlas. For ICEX20, the chosen weights (data-driven) profile derives
 218 from initial CTD casts taken on site, showing an intense warm water intrusion; the baseline
 219 (historical) profile, showing moderate ducted conditions, comes from the average of March
 220 2013 ITP data. This month best matched sea ice and sound speed conditions at the begin-
 221 ning of ICEX20 (Bhatt *et al.*, 2022). It is important to note that all profiles that do show the
 222 Beaufort Lens do so with different local sound speed maxima at different depths, reflective
 223 of the wide range of lens properties observed for all ITP data in the region. The variability

²²⁴ of the lens height and prominence is the main reason an updatable SSP was integrated into
²²⁵ the ICNN solution.

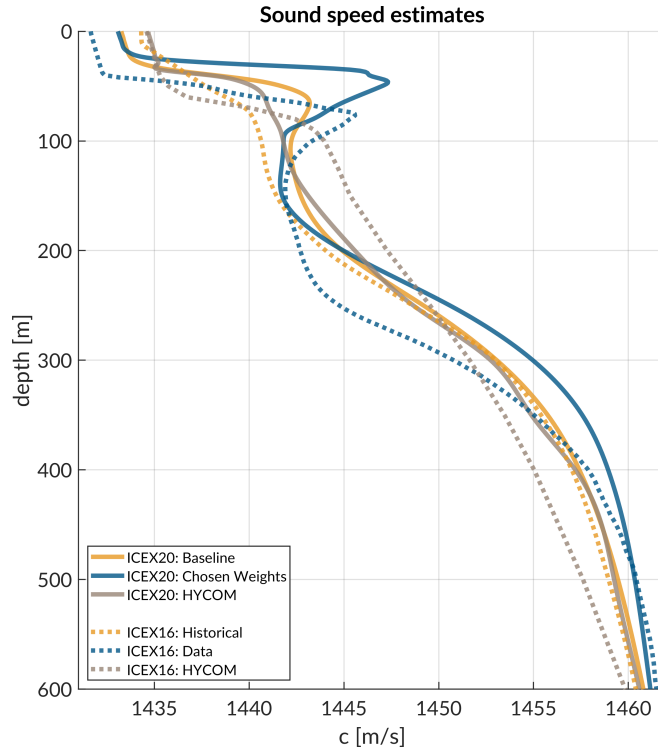


FIG. 3. Sound speed conditions for historical (baseline), data (chosen weights), and HYCOM model for both ICEX16 and ICEX20.

²²⁶ During ICEX20, the HYCOM profile was available but never deployed. For post-
²²⁷ processing comparison, we introduce both the HYCOM profile and an isovelocity case,
²²⁸ 1441.8 ± 3.7 m/s, as the mean and standard deviation of the observed sound speed profile
²²⁹ over the first 200 m. This is a contrived value taken in the style of [Graupe et al. \(2019\)](#)
²³⁰ for the sake of comparison; the default value in the LAMSS simulator, which was not envi-
²³¹ ronmentally informed and used when no updates were available from the ICNN, was 1430
²³² m/s.

233 **III. REAL-TIME PSEUDORANGE ANALYSIS**

234 Because the vehicle’s navigation solution during a mission can only be evaluated on the
235 basis of the error estimates sent, a sister experiment for validating the real-time ranging
236 approach was implemented. Ice buoy modems were run as “virtual vehicles” at a fixed
237 depth, receiving position updates from the other beacons as well as a camp site modem
238 lowered to 20 m. Fig. 4 shows successful events sorted by source depth. In this analysis, we
239 assume there is insignificant displacement between the GNSS puck surface expression and
240 subsurface modem; this is supported by unusually low observed ice drift rates, just 0.7 cm/s
241 on average throughout the mission.

242 **A. Minimal bounce criteria (MBC)**

243 The fundamental challenge to implement GNSS-like navigation, especially in an acousti-
244 cally complex propagation environment, is characterizing a single sound speed to compensate
245 for the effects of ray refraction and reflection. The use of the acoustic modem network for
246 tracking relies on the accurate estimation of travel times between the submerged platform
247 and LBL beacons, supported by clock synchronization and a pre-determined scheduling of
248 acoustic events. For the Beaufort Lens in particular, the strong multipath effects make it
249 virtually impossible to deterministically predict the modem’s detected arrival time.

250 Instead, for each individual receiver i , an embedded stochastic tracking framework is used
251 to provide a running estimate of the effective sound speed $c_{i,j}$ for the conversion from travel
252 time to range from modem j , with the ultimate goal of matching the implied horizontal

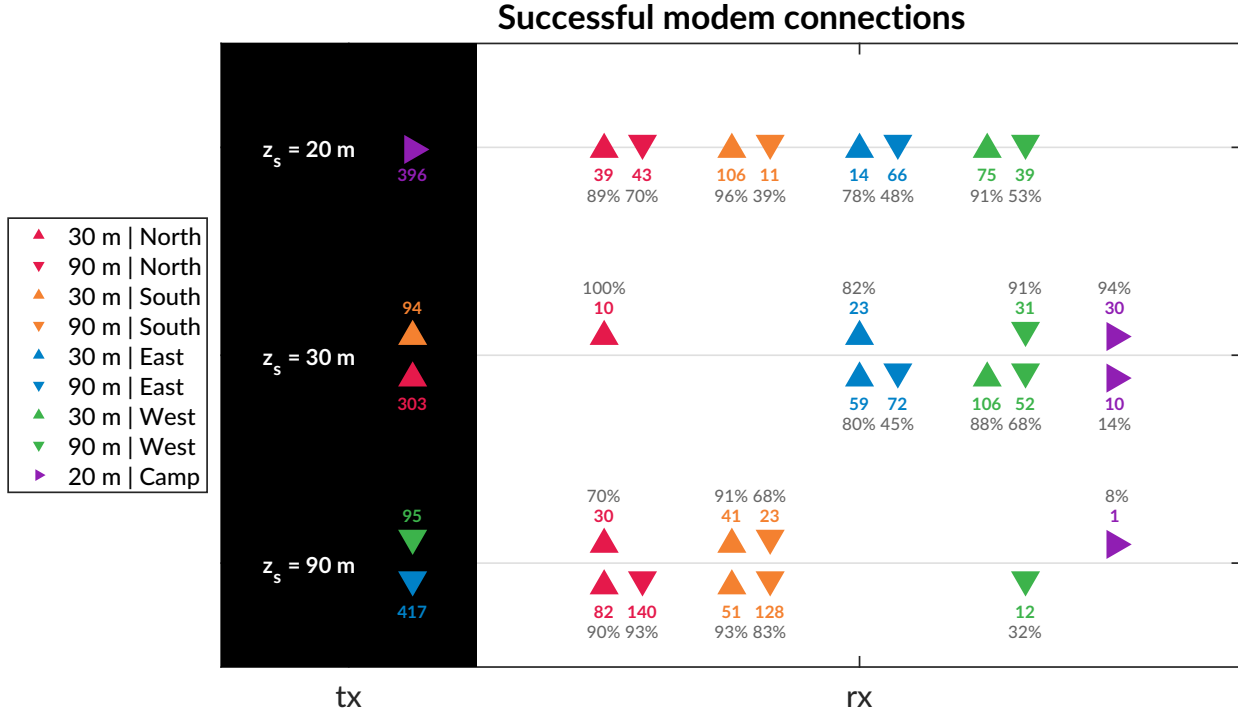


FIG. 4. An overview of the modem experiment by source and receiver depth and position. The black column on the left, *tx*, shows the source depth, z_s , with the total number of transmissions. The column on the right, *rx*, shows the receivers with the number of successful decodings and the percent success rate, defined as the ratio of decoded to detected. The orientation of the triangles—sideways, upwards, and downwards—corresponds to depths of 20, 30, and 90 m.

253 effective sound speed, i.e., the GPS-recorded distance between two nodes divided by the
 254 modem-recorded one way travel time between them.

255 In the ICEX20 configuration, the acoustic tracker is running on the topside computer,
 256 which controls the ICNN. Here we assume that the effective sound speeds $c_{i,j}$ are smoothly

257 varying over the course of a vehicle mission, i.e., with respect to range from signal origin at
 258 transmitter j , mission time, and the thirty-second frequency.

259 When the topside tracking framework receives a message, with a time delay, Δt , it will
 260 request a new estimate for $c_{i,j}$ along with its standard deviation. The effective sound speed
 261 is predicted using the vehicle's reported depth and the extrapolated navigation solution for
 262 range, \hat{r} , as inputs to the ray tracing program, which returns an impulse response estimate
 263 in the form of ray travel times dt_j and amplitudes a_j .

264 The initial call to BELLHOP is over a local grid centered at the range and depth posited
 265 by the onboard tracking solution. The grid, compared to a point solver, adds redundancy
 266 in resolving the actual multipath structure for a reliable acoustic path without overtaxing
 267 onboard computational time and memory. It is initialized as 11×11 points spanning 10
 268 m horizontally and 20 m vertically. The horizontal dimension reflects the accumulated
 269 vehicle position error given a thirty-second communication cycle; the vertical dimension
 270 reflects how, computationally, eigenrays of the same timefront seem to stack vertically in
 271 the water column. For each grid point, BELLHOP produces a number of arrivals resulting
 272 from multiple propagation paths. Using only the N_0 rays with neither surface nor bottom
 273 bounces, the tracking system will then estimate the current effective sound speed c from a
 274 power weighted average of the ray travel times,

$$c = \frac{\hat{r} \sum_{n=1}^{N_0} a_n^2}{\sum_{n=1}^{N_0} dt_n a_n^2}, \quad (1)$$

275 and the associated weighted standard deviation,

$$\sigma_c \simeq \sqrt{\frac{\sum_{n=1}^{N_0} (dt_n - \hat{r}/u)^2 a_n^2}{\sum_{n=1}^{N_0} a_n^2}} \frac{u^2}{\hat{r}} \quad (2)$$

²⁷⁶ If no direct paths exist, i.e. $N_0 = 0$, then the effective speed is computed using the same
²⁷⁷ algorithm for the ray arrivals with one bounce, and so on.

²⁷⁸ Finally, the pseudorange is calculated simply as

$$r_{i,j} = c_{i,j} \Delta t_{i,j} \quad (3)$$

²⁷⁹ Thus the minimal bounce criteria (MBC) assumes the signal detected by the modem will
²⁸⁰ be dominated by a set of paths with the least number of boundary interactions. Impor-
²⁸¹ tantly, this stochastic, ensemble method for group velocity calculation can run in real-time,
²⁸² appearing to be orders of magnitude faster than other post-processing methods which seek
²⁸³ to determine the specific ray itself that best matches a prominent indicator from the arrival
²⁸⁴ structure. The BELLHOP simulation that runs this calculation uses 3600 rays with launch
²⁸⁵ angle fan of -60 to 60 degrees, a representative depth dependent sound speed profile, and a
²⁸⁶ range dependent bathymetry.

²⁸⁷ **B. Pseudorange error metrics**

²⁸⁸ The sister modem experiment generated 811 beacon to beacon communication events
²⁸⁹ with their own real-time MBC group velocity predictions. Given the complexity of the
²⁹⁰ ICNN system, this experiment did not collect an exhaustive set of data across all buoy,
²⁹¹ source depth, receive depth, and model sound speed combinations. The algorithm generally
²⁹² overestimates pseudoranges because it resolves the effective sound speed for the most direct
²⁹³ path.

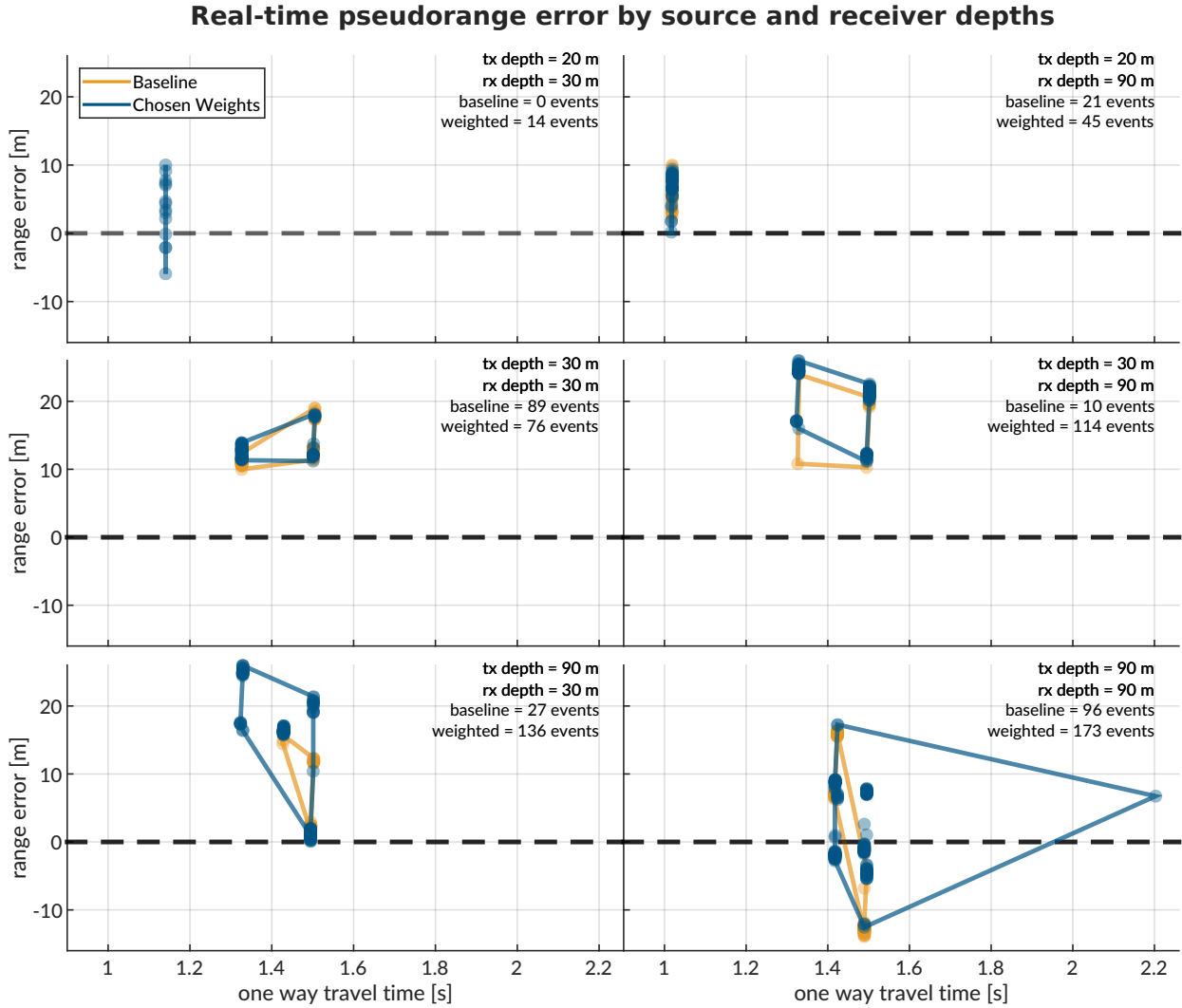


FIG. 5. The real-time range error by source (rows: 20, 30, and 90 m) and receiver (columns: 30 and 90 m) pairings for both sound speed estimates used during ICEX20. The amount of communication events is notated in the top right of each panel. The dashed line indicates no range error, and the boundary drawn indicates scope of the range error as a function of one way travel time.

²⁹⁴ Fig. 5 shows the range error boundary for both SSP inputs used in ICEX20. A promising
²⁹⁵ sign that the MBC method adapts sound speed somewhat intelligently is the lack of error
²⁹⁶ growth as travel time increases. The baseline SSP ($n=243$ events) has an absolute pseudor-

297 ange error of 11.38 ± 4.23 m; the weighted SSP ($n=568$), 11.36 ± 8.12 m. The discrepancy
 298 between these two is largely due to outlier events only contained in the weighted SSP set.
 299 Where there is overlap between sound speed conditions used for the real-time MBC, the
 300 pseudorange error difference is no more than a few meters. The overarching results show
 301 that sound speed estimates derived from eigenrays for a local grid, as opposed to a singular
 302 point, are accurate enough to support vehicle navigation. While the MBC looks for just the
 303 least complex multipath, the high density of launch angles almost always guarantees a direct
 304 path for the beacon-to-beacon configurations. Nonetheless, the consistent overestimation of
 305 pseudorange invites further analysis into acoustic arrival matching.

306 C. Eigenray identification for beacon-to-beacon events

307

308 Accounting for ice movement between beacons creates nominal ranges with small vari-
 309 ability. Figs. 6, 7, and 8 show eigenrays for three sound speed environments for source
 310 depths of 20, 30, and 90 m, respectively. Eigenrays were initially found using the built-in
 311 BELLHOP protocol with a launch angle fan of 2400 rays between -60 and 60 degrees. Sepa-
 312 rately, recorded travel times between beacons were clustered with 1 millisecond boundaries
 313 such that some source-receiver pairs had multiple, distinct travel times to approximate. The
 314 BELLHOP eigenray returns were then filtered such that one was selected per travel time
 315 cluster, in the hopes that the eigenray will converge to the receiver locations for the most
 316 realistic sound speed input. It should be noted that bottom bounces were recovered but

³¹⁷ filtered out. The three source depths create distinct ray geometries with respect to the three
³¹⁸ sound speed inputs.

³¹⁹ **1. Source depth of 20 m**

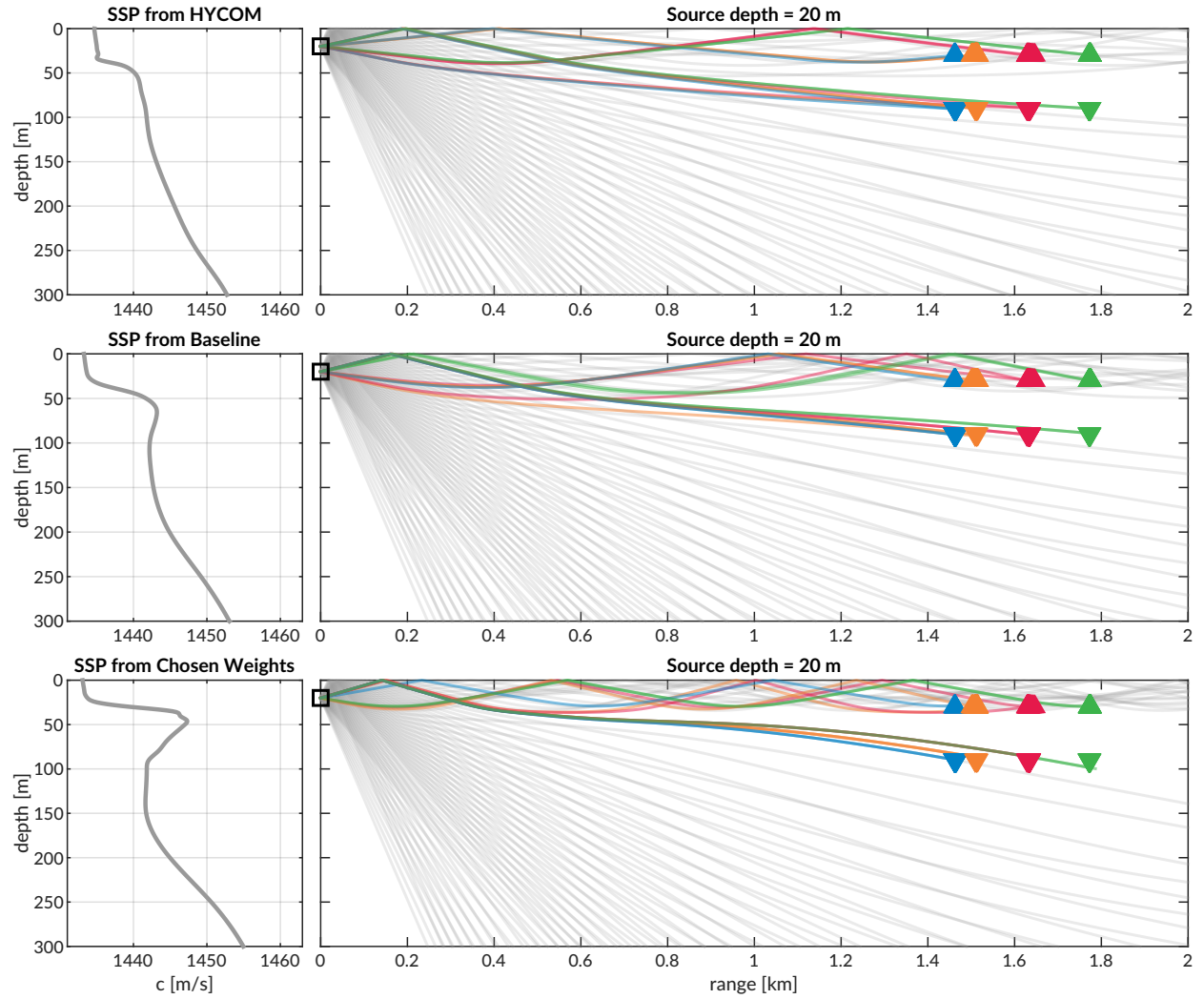


FIG. 6. Eigenrays for beacon-to-beacon events for each sound speed with a nominal source depth of 20 m over a total ray fan in gray. The beacons are highlighted in color/marker coding in Fig. 4.

320 For a source at 20 m in depth, shown in Fig. 6, reliable eigenrays are found for all sound
 321 speed inputs. Rays refract upwards and neatly intersect with the shallow and deep receiver
 322 locations between 1.5 and 1.8 km in range. However, the ray paths for the shallow receivers
 323 change both in the number of surface interactions and where the surface interactions occur
 324 with respect to range across the SSPs. As the Beaufort Lens strengthens, the chosen paths to
 325 the second farthest shallow buoy (North, in red) interact with the surface more and become
 326 distinct. The weighted SSP shows the most interesting effects for the deeper receivers. The
 327 ray paths all interact with the surface and the eigenrays for the Northern (red) and Western
 328 (green) buoys are in fact the same ray.

329 *2. Source depth of 30 m*

330 The ray geometries from the 30 m source, shown in Fig. 6, show a similar degradation
 331 of eigenray identification with increased ducting. Receptions span 1.5 to 3.2 km. Once
 332 again, eigenrays for HYCOM and the baseline SSP are visually appropriate. Rays for the
 333 weighted SSP show how the surface channel intensifies ice interactions and how the shadow
 334 zone denies reliable acoustic paths. Pointedly, the increasing number of surface reflections to
 335 the farthest shallow buoy (North, in red) crystallize the MBC's tendency for overestimation.
 336 For the HYCOM, baseline, and weighted SSP inputs, the most appropriate eigenrays show
 337 2, 3, and 4 surface interactions.

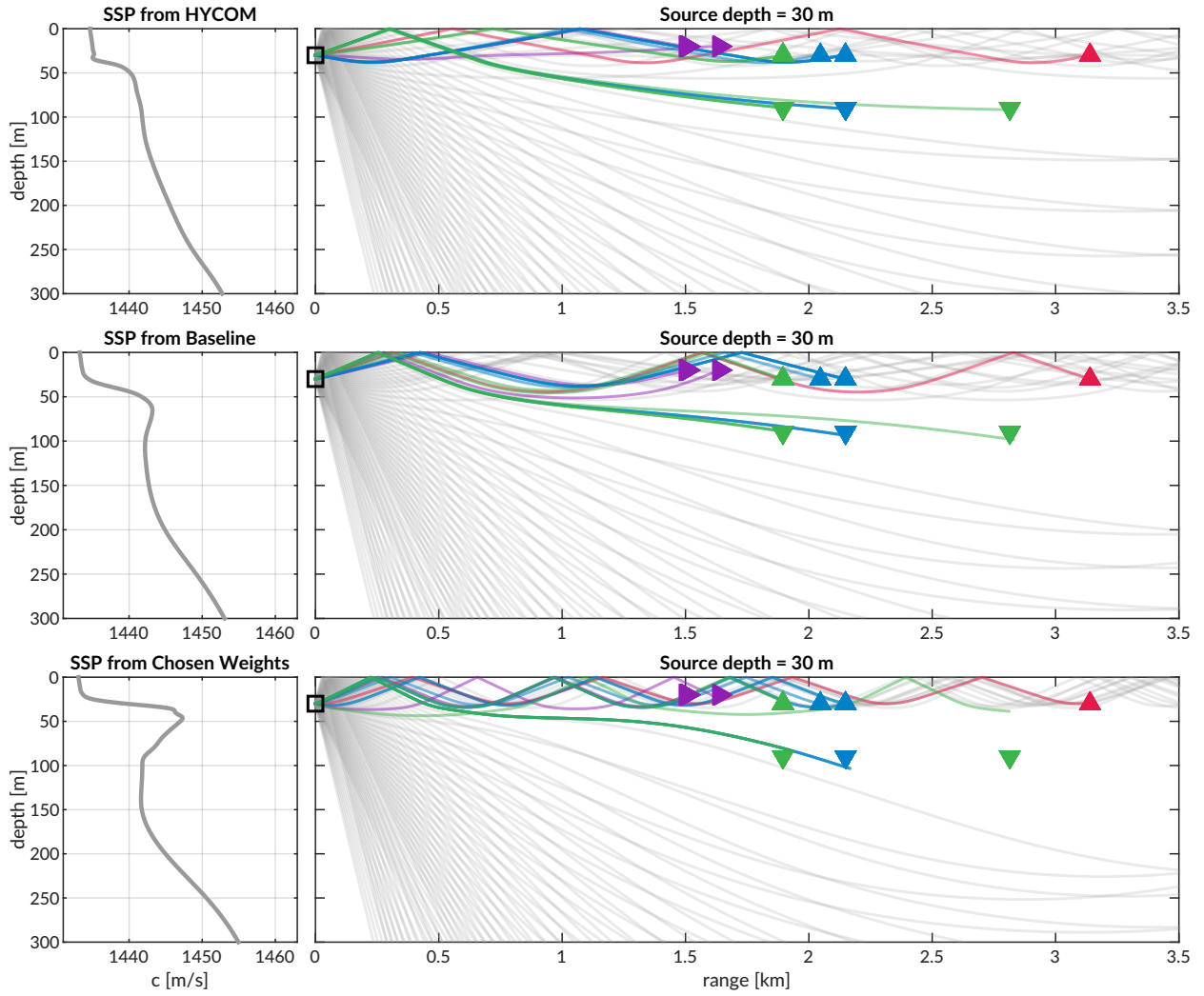


FIG. 7. Eigenrays for beacon-to-beacon events for each sound speed with a nominal source depth of 30 m over a total ray fan in gray. The beacons are highlighted in color/marker coding in Fig. 4.

³³⁸ **3. Source depth of 90 m**

³³⁹ Lastly, Fig. 8 shows ray geometries from the 90 m source, elucidating a different extent
³⁴⁰ of the shadow zone. While the receiver locations are similar to that of the 30 m source
³⁴¹ depth, the deeper source depth effectively negates the upper duct and places the upper (and
³⁴² some of the lower) receivers in unreliable acoustic paths. The HYCOM eigenrays still show

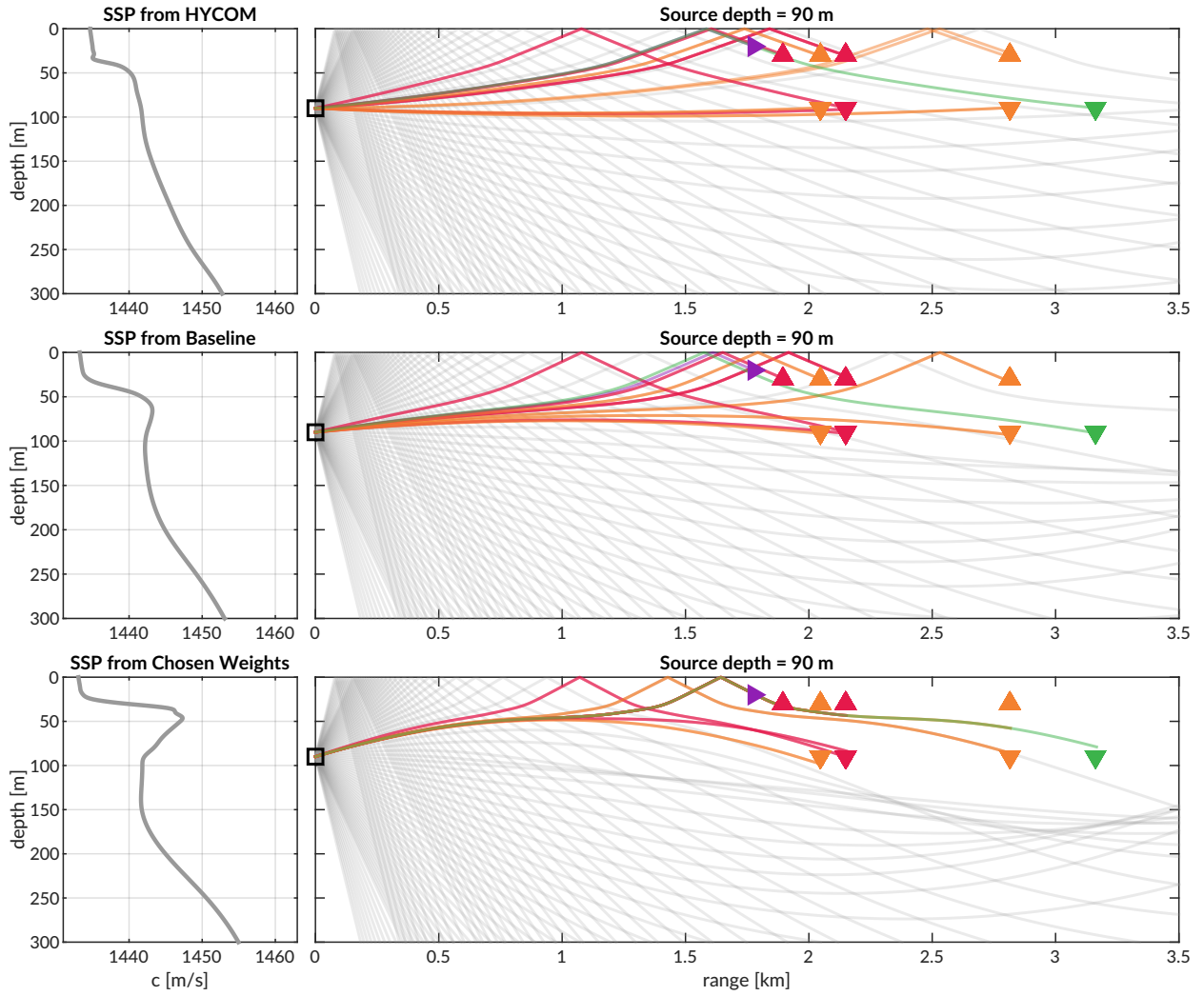


FIG. 8. Eigenrays for beacon-to-beacon events for each sound speed with a nominal source depth of 90 m over a total ray fan in gray. The beacons are highlighted in color/marker coding in Fig. 4.

343 the most reliable acoustic paths that deteriorate with increasing ducted conditions. The
 344 lack of direct paths from the observed SSP further points out the shortcomings of the MBC
 345 approach.

346 The goal of the MBC algorithm was to provide a reliable, physically intuitive interpre-
 347 tation of the acoustic propagation without taking on the additional burden of regularly
 348 identifying specific paths that may connect any given source-receiver pair in the network.

³⁴⁹ While it was unlikely to resolve multipath arrivals that triggered successful modem detection,
³⁵⁰ an isovelocity approach would have provided no adaptivity against source and receiver
³⁵¹ depth differences. Its performance was adequate for vehicle navigation and would have likely
³⁵² sufficed if it were not for the prominence of the duct observed relative that of other model
³⁵³ and data products.

³⁵⁴ **IV. POST-PROCESSED PSEUDORANGE ANALYSIS**

³⁵⁵ From all events recorded during the modem test experiment, there are 1242 successfully
³⁵⁶ decoded beacon-to-beacon events. Thus, a post-processing analysis that emulates the real-
³⁵⁷ time navigation engine was run to overcome the unequal distribution of communication
³⁵⁸ events with respect to depth, range, and sound speed status.

³⁵⁹ It is important to note that the value for the extrapolated range, \hat{r} , is only tracked by
³⁶⁰ topside for a modem claiming to be the vehicle; thus we replace \hat{r} with the GPS-tracked range
³⁶¹ for all modem events. Because \hat{r} converges to the correct solution, a comparison of \hat{r} with
³⁶² the GPS-tracked range shows a normal, zero-centered distribution within the bounds of GPS
³⁶³ drift. The analysis therefore seeds realistic but “omniscient” knowledge of the extrapolated
³⁶⁴ range and emulates the post-processing pipeline to more thoroughly evaluate the acoustic
³⁶⁵ pseudorange estimate for all modem events. Sound speed inputs are the isovelocity sound
³⁶⁶ speed in addition to the modeled, baseline, and weighted SSPs from Fig. 3. The analysis
³⁶⁷ replicates the MBC but also introduces a new filtering algorithm, the nearest bounce criteria
³⁶⁸ (NBC), based on insights gleaned from the eigenray analysis. Accordingly, the results in
³⁶⁹ this section evaluate the utility of the algorithms and sound speed sources, divorced from
³⁷⁰ their role in the ICNN while maintaining real-time relevance.

³⁷¹ **A. Nearest bounce criteria (NBC)**

³⁷² The extent of ray bending and repeated reflections is extremely dependent on the degree
³⁷³ of the Beaufort Lens observed. Based on this insight, a new algorithm, the nearest bounce

³⁷⁴ criteria (NBC), is a slight modification from the MBC and includes multipath as a new
³⁷⁵ dimension of information to exploit. This metric, while run in post-processing, adds a
³⁷⁶ negligible amount of computation for real-time efficacy.

³⁷⁷ Given a running estimate for the effective sound speed $c_{i,j}$ between nodes i and j , the
³⁷⁸ navigation system has an extrapolated value for range, \hat{r} , and a recorded travel time, $\Delta t_{i,j}$.
³⁷⁹ Instead of using only the N_0 rays with neither surface nor bottom bounces to estimate
³⁸⁰ conversion speed, and subsequently moving to incremental number of bounces only when no
³⁸¹ valid direct path solutions exist, we solve for the power weighted average of the ray travel
³⁸² time for the N_k rays with k bounces,

$$t_k = \frac{\sum_{n=1}^{N_k} dt_n a_n^2}{\sum_{n=1}^{N_k} a_n^2}, \quad (4)$$

³⁸³ find the nearest matching power weighted average to recorded travel time,

$$t_{i,j,k} = \min_{k=0,1,2,\dots} |t_k - \Delta t_{i,j}| \quad (5)$$

³⁸⁴ predict an effective sound speed,

$$c_{i,j} = \frac{\hat{r}}{t_{i,j,k}} \quad (6)$$

³⁸⁵ and estimate the range as was done previously.

$$r_{i,j} = c_{i,j} \Delta t_{i,j} \quad (7)$$

³⁸⁶ Whereas the MBC outputs a scalar, this method first outputs a vector of effective sound
³⁸⁷ speeds based on the number of reflections. Then a single value is selected that best matches
³⁸⁸ the recorded travel time, as the detected arrival is not always the first arrival or the direct
³⁸⁹ path and could even be masked by noise or blocked temporarily ([Deffenbaugh *et al.*, 1996b](#)).

³⁹⁰ We manually cap the number of bounces at four because of the smaller operational scale and
³⁹¹ the attenuation accrued with many surface interactions. Bottom bounces are not encoded
³⁹² separately because of ray's tendency to refract upward, not due to information limitations.

³⁹³ **B. Effective sound speed predictions**

³⁹⁴ The minimal and nearest bounce algorithms are applied with the three sound speed inputs
³⁹⁵ shown in Figs. 6, 7, 8. The resulting predicted effective sound speeds are shown in Fig. 9
³⁹⁶ for all source depths versus one way travel time.

³⁹⁷ The goal of the effective sound speed prediction is to converge towards the implied sound
³⁹⁸ speed, i.e. the GNSS-derived range divided by the recorded travel time. As the environ-
³⁹⁹ mental and ray filtering method become better representations of the real ocean, the lower
⁴⁰⁰ the expected mismatch is between the implied and estimated effective sound speeds.

⁴⁰¹ The various sound speed inputs—isovelocity aside—not only modify the predicted effec-
⁴⁰² tive sound speed, as seen by the colored vertical offsets, but often classify a distinct number
⁴⁰³ of bounces. HYCOM sees the most direct and one bounce multipath structures, lending a
⁴⁰⁴ bias for faster speeds; the weighted SSP sees the most double and triple bounces, favoring
⁴⁰⁵ slower speeds; the baseline sound speed exists in between. Very rarely is the multipath
⁴⁰⁶ structure classified as a direct path, i.e., where the NBC defaults to the MBC prediction. In
⁴⁰⁷ fact, the higher the multipath classification, the more accurate the sound speed prediction
⁴⁰⁸ is, likely driven by a tighter or even sparser bundle of rays. Discontinuities in multipath
⁴⁰⁹ classification provide initial evidence for its importance to a smoothly varying group velocity,
⁴¹⁰ as shown in the cluster of 30 to 30 m transmissions in Fig. 9, where HYCOM jumps from

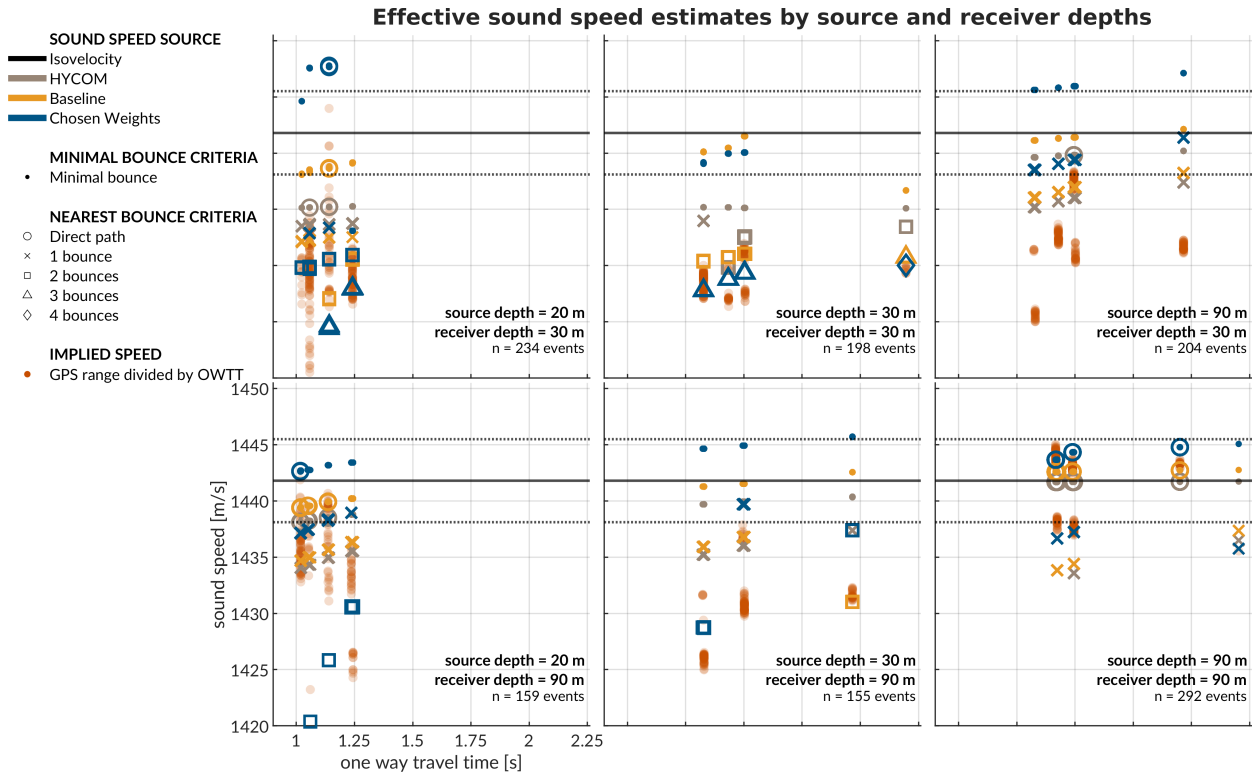


FIG. 9. A post-processing comparison of effective sound speed predictions for all beacon-to-beacon events. The rows share receiver depth; the columns share source depth. The recorded travel time is on the x-axis and the predicted effective sound speed is on the y-axis. The sound speed source is indicated by color. The isovelocity is shown as the mean \pm the standard deviation. The minimal and nearest bounce criterion are distinguished by different marker shapes, compared to the separately colored red dots showing the implied calculation.

411 one to two classified bounces amidst the baseline SSP and weighted SSP smoothly increasing
 412 while consistently seeing two and three classified bounces, respectively. Of course, the
 413 prediction deteriorates with cross-layer transmissions across the duct, but not to the same
 414 degree at which eigenrays could not be found for the weighted SSP in section III C. The

⁴¹⁵ evidence suggests that the grid based method provides a useful amount of redundancy to
⁴¹⁶ resolve similar enough eigenrays.

⁴¹⁷ It is useful to think about in what case the isovelocitity—or any isovelocitity framing—would
⁴¹⁸ have been appropriate. The transmissions from shallow to shallow receiver may have
⁴¹⁹ matched the default configuration of 1430 m/s. The isovelocitity contrived for this paper,
⁴²⁰ 1441.8 m/s, best matches the transmissions from 90 to 90 m. The one from [Graupe *et al.*](#)
⁴²¹ ([2019](#)), 1450 m/s, would have had a systemic overestimation. In addition, over the course
⁴²² of the four day experiment, the local maxima of the Beaufort Lens changed from roughly
⁴²³ 1447 m/s at 40 m to 1442 m/s at 60 m. Given that implied sound speeds just for beacon-
⁴²⁴ to-beacon events span 1420 to 1445 m/s, it is safe to say that a nominal sound speed would
⁴²⁵ sacrifice pseudorange accuracy somewhere, and that an adaptive approach is necessary even
⁴²⁶ for short and/or small scale operations in the Beaufort Lens.

⁴²⁷ C. Pseudorange error metrics

⁴²⁸ Pseudorange estimation plays an important role in trilateration. Fig. [10](#) shows the
⁴²⁹ directional pseudorange error “footprints” for the four sound speed inputs with the NBC
⁴³⁰ approach, separated by source and receiver depth configurations.

⁴³¹ The weighted SSP range error generally has the smallest and most zero-centered footprint.
⁴³² The one case it does not is for the source-receiver pairings between 30 and 90 m in depth. The
⁴³³ increased error for these is most likely driven by the computational artifacts encountered
⁴³⁴ when propagating through the steep sound speed gradients of the lens and through the

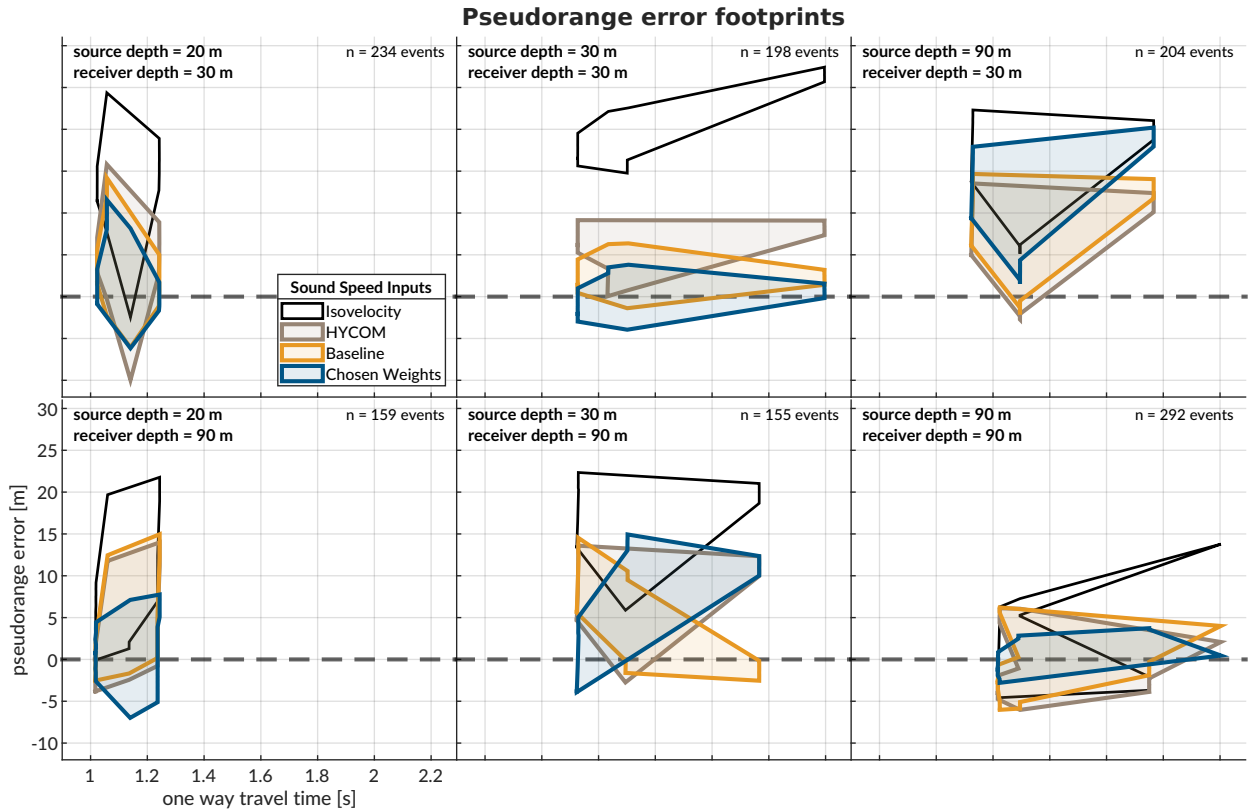


FIG. 10. The post-processed pseudorange error; the rows share receiver depth; the columns share source depth. The dashed gray line shows no error. The shaded region connects the range performance across all events.

⁴³⁵ shadow zone. All other source depth pairings are significantly improved using the chosen
⁴³⁶ weights compared to HYCOM or the baseline.

⁴³⁷ When using a linear scaling to convert travel time into range, any offset between the
⁴³⁸ assumed sound speed and the horizontal group velocity produces unconstrained error with
⁴³⁹ increasing receiver distance, whereas an adaptive estimate would exhibit no such trend. This
⁴⁴⁰ is easily observed in the same-layer links, i.e., 30 to 30 m and 90 to 90 m. In cross-layer
⁴⁴¹ links, the isovelocity does not perform better but tends to exaggerate or flip the footprint
⁴⁴² created adaptively.

443 The improvement from MBC to NBC is most evident for the data-driven sound speed;
444 while the HYCOM SSP improves from a median absolute range error of 6.41 to 4.61 m,
445 the baseline SSP improves from 10.30 to 2.27 m, and the weighted SSP improves from
446 13.28 to 2.12 m. In comparison, the isovelocity has a median error of 13.09 m. The order
447 of magnitude improvement in the ducted SSPs demonstrate the effectiveness of the NBC
448 algorithm exploiting the observed multipath conditions.

449 There is one example that helpfully illustrates the improvement brought upon by bounce
450 classification. For transmissions between North and South at 30 m, the OWTT spread is
451 2.1958 to 2.1963 s; the GNSS-tracked distance is 3138.54 to 3140.87 m; and the implied
452 effective sound speed is 1429.3 to 1430.1 m/s. For these transmissions, the weighted SSP
453 and the MBC approach produce a pseudorange error of -1491 m, as the effective sound speed
454 is dominated by bottom bounce arrivals with much greater travel times. The NBC approach
455 categorizes this same record as a quadruple surface bounce, reducing the pseudorange error
456 to less than a meter. Comparatively, the NBC approach for HYCOM and the baseline
457 SSP produce pseudorange errors of 8.30 and 2.39 m, respectively. There is strong evidence
458 to suggest that the sound speed and multipath fidelity codependently improve localization
459 accuracy.

⁴⁶⁰ **V. TRILATERATION FOR ICEX20 FIELD DATA**

⁴⁶¹ To overcome potentially intermittent acoustic communication, the operational paradigm
⁴⁶² of the ICNN computes corrections relative to the trilaterated position estimates transmitted
⁴⁶³ by the vehicle, rather than transmitting the updated positions themselves. The reliability of
⁴⁶⁴ the correction is directly linked to how accurately the travel time measurements are converted
⁴⁶⁵ to pseudoranges. This section aims to resolve that tension by reevaluating the trilateration
⁴⁶⁶ results with respect to the MBC and NBC algorithms. The MBC/NBC effective speed
⁴⁶⁷ predictions were tracked independently for each source-receiver pair; although the sound
⁴⁶⁸ speed was expected to be locally smooth near a given receiver, no such assumption was
⁴⁶⁹ enforced between distinct acoustic links.

⁴⁷⁰ **A. Re-positioning beacon to beacon events**

⁴⁷¹ When the beacons ran as virtual vehicles, the ICNN did not have access to that buoy's
⁴⁷² GPS data stream except for what was sent via digital acoustic message. The static nature of
⁴⁷³ the experiment means that the initial estimate transmitted to the ICNN was in fact a ground
⁴⁷⁴ truth position. Therefore, a distribution of corrections from the ICNN, as shown in Fig. 11,
⁴⁷⁵ reflects positioning accuracy. The NBC clearly outperforms the MBC, with almost 80% of
⁴⁷⁶ the corrections below 6 meters and the median within the deployed GNSS puck precision
⁴⁷⁷ of 3 meters. By contrast, the MBC shows roughly 20% within the GNSS puck precision,
⁴⁷⁸ and separate peaks from 9–12 meters and 21–27 meters. This trimodal nature reflects the
⁴⁷⁹ distribution of reflections on the ice surface.

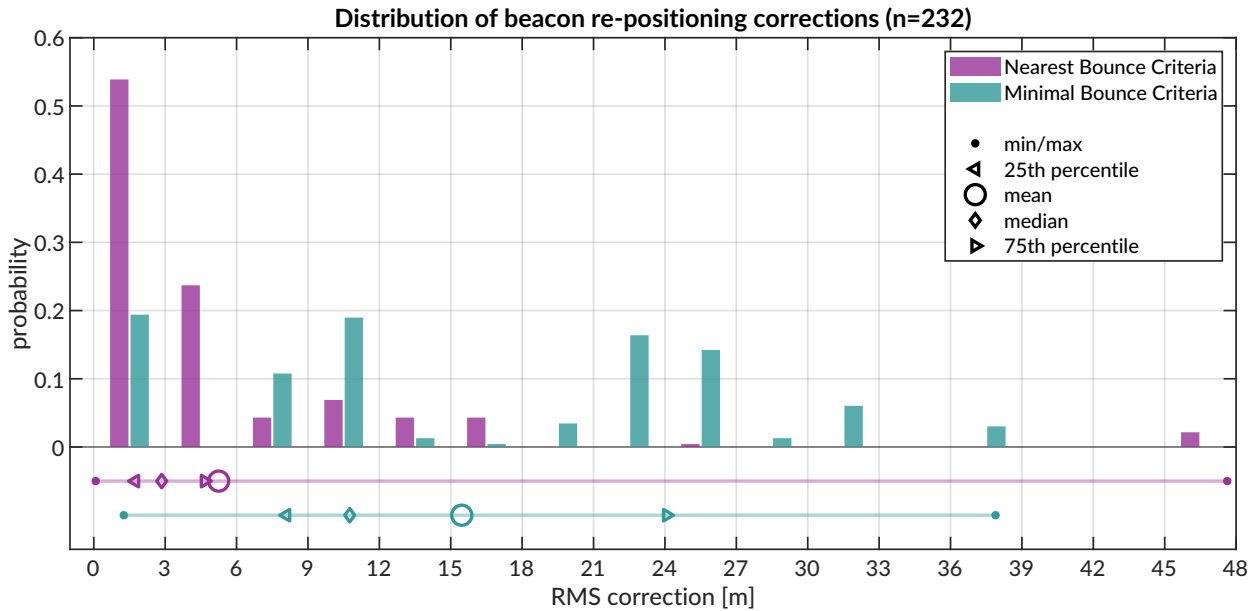


FIG. 11. Trilateration events; however, 264 entries are 2-beacon solutions, 22 are 3-beacon, and 2 are 4-beacon. When limited to only two ranging circles, the trilateration chooses the closer of the two intersection points. The x-axis is cut off at the upper limit for the NBC algorithm.

480 In several events, the MBC is unable to accurately estimate the effective sound speed for
 481 one of the acoustic links, leading to a large positioning error. The NBC, however, better
 482 resolves an approximation of the acoustic path. For example, in some trilateration solutions
 483 for the Eastern buoy, the MBC shows a correction of more than a kilometer; the NBC is
 484 two orders of magnitudes less.

485 **B. Re-navigating AUV *Macrura***

486 Up to this point, pseudorange estimation and localization have been evaluated on GPS-
 487 linked beacon-to-beacon connections to validate the NBC algorithm. This analysis ports the
 488 MBC and NBC algorithms to re-navigate the AUV *Macrura*.

489 In comparison to the modem experiment, the AUV data clearly exhibit instances where
490 a receiver detects the same transmission more than once. This is not surprising considering
491 the complex multipath provided by the Beaufort Lens. The 11 hour vehicle mission con-
492 tains 3,260 transmissions, 12,938 total detections, and 4,704 successful receptions. Allowing
493 receptions with PSK errors would almost double the number of recorded multipath arrivals
494 exploited for positioning, if a real-time solution could correctly parse paths from different
495 arrivals in the same thirty-second cycle. Thus it remains a future endeavor to explore how
496 failure mode information from acoustic modems could be used to identify unsuccessful but
497 otherwise trustworthy arrivals to augment trilateration samples.

498 The following performance analysis is constrained to what the vehicle acted on in real-
499 time. AUV *Macrura* and the ICNN ran an adaptive depth behavior to maintain acoustic
500 communication on the insight that cross-layer links were more likely to fail than same-layer
501 ones. Accordingly, the vehicle dove deeper than 50 meters about 20% of the time it was
502 underway.

503 In contrast to the modem tests, where position correction illustrated re-positioning ac-
504 curacy, the re-navigation corrections are less valuable in the absence of GNSS ground truth.
505 The correction magnitude necessarily depends on the vehicle's internal navigation estimate,
506 which is prone to larger errors from sensor drifts, ocean currents, and other error not cap-
507 tured in the hydrodynamic model. Thus, larger corrections are not necessarily indicative of
508 worse performance. Navigation accuracy is better described by trilateration error, the RMS
509 of the remaining pseudorange errors from each acoustic link.

510 Fig. 12 shows the correction magnitudes and trilateration errors for events with three or
 511 more receptions during AUV operations. Whereas the MBC has a fairly bimodal nature,
 512 with peaks centered around 10–15 and 35–40 m, the NBC favors smaller corrections, from
 513 5–20 m, and has a long tail. The distribution of corrections are much larger than the
 514 distribution of RMS error. It is apparent that, while both methods are quite successful,
 515 there is strong evidence that the NBC achieves single meter accuracy.

516 C. Investigating potential GNSS noise

517

518 The fact that the bulk of the best performing re-navigation error exists within the preci-
 519 sion of the GNSS unit deployed invites a further look into GNSS noise. In the Arctic, GNSS
 520 performance worsens due to poor constellation coverage, larger ionospheric effects, and mul-
 521 tipath interference (Gwal and Jain, 2011; Jung *et al.*, 2018; National Research Council, 2011;
 522 Reid *et al.*, 2016; Swarlund *et al.*, 2016; Themens *et al.*, 2015). Radio infrastructure that
 523 provides position corrections and references does not regularly extend to polar regions. The
 524 effect is minor for surface platform navigation —roughly 15 m of horizontal precision has
 525 been displayed at the North Pole—but is significant enough to register against the modem’s
 526 detected travel times. Fig. 13 zooms in on the GNSS and OWTT noise relative to the ice
 527 movement for two pairs of modem buoy connections. The two panels indicate the GPS drift
 528 as $\delta R = \sqrt{\delta x^2 + \delta y^2}$ and temporal drift, δt , relative to the median OWTT recorded between
 529 the two modems. The dashed line is scaled by a group velocity of 1440 m/s, such that if

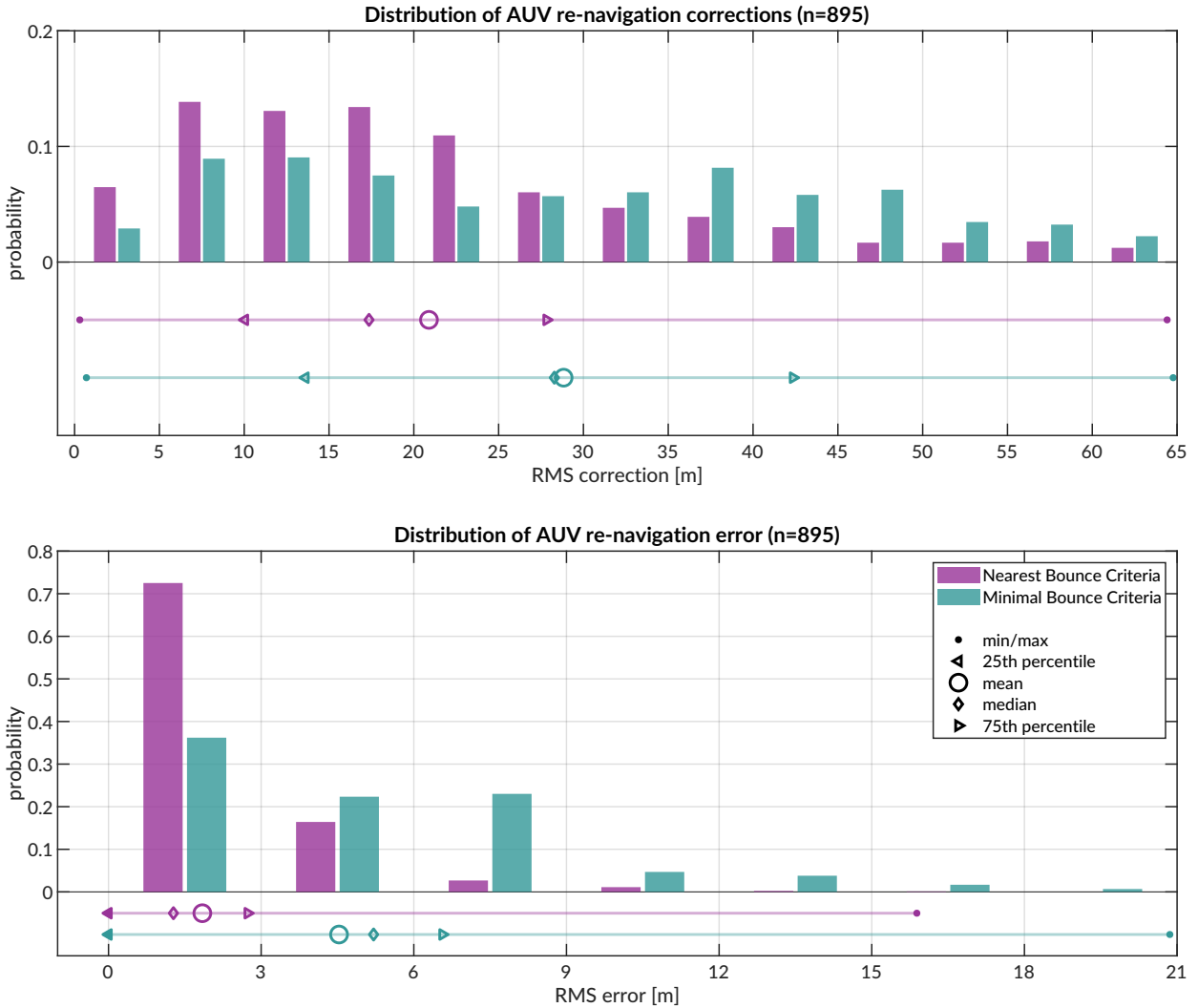


FIG. 12. Distribution of vehicle re-navigation corrections (top) and error (bottom) computed in post-processing for the Minimum and Nearest Bounce Criterion.

530 there were ideal sensor measurements with no drift, all events should exist on or near the
 531 line.

532 The top panel shows the connections between the North and East buoys. The clusters
 533 scaling along the 1440 m/s guideline suggest relative ice movement picked up by both GNSS
 534 and OWTT. But the vertical distribution across many arrival time bands is indicative of

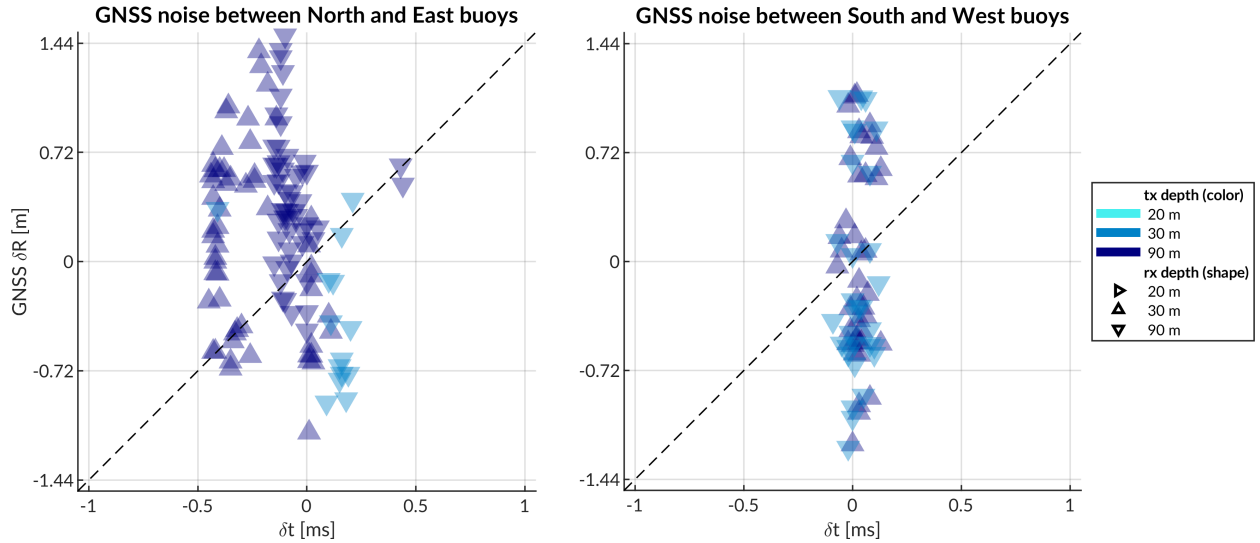


FIG. 13. A comparison of GPS drift (y-axis) versus OWTT drift (x-axis) for corners of the ICNN network with different source depths.

535 the GNSS fluctuations in precision, or noise. Some minor offsets between these vertical
 536 bands relate to different operational configurations of source and receiver depth. The idea
 537 of GNSS noise relative to OWTT is further indicated by events between two other buoys,
 538 South and West. The relatively thin time window suggests these buoys are moving in
 539 a more rigid ice floe and that there is minimal impact by source and receiver depth on
 540 the spread of OWTT. Yet, the vertical distribution, spanning almost 4 meters, cannot be
 541 explained by time differentials due to acoustic scattering, multipath, and/or environmental
 542 microstructure. This conclusion corroborates the vertical spread of implied effective speeds
 543 in Fig. 9.

⁵⁴⁴ **VI. DISCUSSION**

⁵⁴⁵ Underwater navigation research is broadly motivated by acquiring GNSS-like navi-
⁵⁴⁶ gation in GNSS-denied conditions. Accurate range estimation is essential to mitigating error.
⁵⁴⁷ Current approaches for underwater acoustic navigation simplify the non-linear relationship
⁵⁴⁸ between a SSP and timefronts with a deterministic sound speed. Thus, the conversion of
⁵⁴⁹ travel time into distance can be pre-conditioned for error and error growth over the course
⁵⁵⁰ of a vehicle mission. This work introduces a lightweight stochastic prediction of an effec-
⁵⁵¹ tive sound speed along the path between source and receiver, retooling arrival methods
⁵⁵² generally deemed too complex or labor intensive for real-time. We assume that the effec-
⁵⁵³ tive sound speed would be a locally smoothly varying function with respect to operational
⁵⁵⁴ conditions—horizontal and vertical differences and rate of difference between source and re-
⁵⁵⁵ ceiver. The field-tested approach, the minimal bounce criteria, facilitated a successful AUV
⁵⁵⁶ recovery in a total ice-covered, double ducted environment. The accuracy of the MBC was
⁵⁵⁷ validated against GPS-linked beacon-to-beacon communications. Given a consistent bias
⁵⁵⁸ towards overestimation, an improved algorithm, the nearest bounce criteria, was developed
⁵⁵⁹ on the insight that multipath structure may play an outsized role in maintaining a smoothly
⁵⁶⁰ varying effective sound speed. The NBC was developed with field data and reevaluated on
⁵⁶¹ vehicle data, achieving a position accuracy and precision that rivals that of the deployed
⁵⁶² GNSS puck.

⁵⁶³ A key insight for both approaches was seeking an eigenray ensemble around an estimated
⁵⁶⁴ location instead of seeking to unambiguously match arrivals. The ensemble diversified the

565 simulated multipath possibilities to better capture the actual multipath recorded. In this
566 way, the solution exploits multipath, generally viewed as a source of uncertainty, as a new
567 dimension of information to improve localization accuracy. Based on the navigation and re-
568 navigation results of our AUV deployment in the ice-covered Beaufort Sea, we conclude that
569 embedding a model-aided prediction of the effective sound speed has an outsized benefit
570 to minimizing trilateration error, and that our approach sufficiently resolves the acoustic
571 timefronts for an unpredictable, complex propagation environment like the double ducted
572 Beaufort Lens.

573 There are many avenues through which this approach can be further refined and tested for
574 field operations. Amongst them is defining the uncertainty grid for BELLHOP via stochastic
575 or data-driven measures such as the distance traveled by the AUV between ICNN updates
576 or the magnitude of the position corrections by the ICNN. Another is to entirely remove the
577 seeded range and instead rely on the submerged asset's depth and recorded OWTT to find
578 high probability fields in range.

579 The relatively simple nature of this approach suggests it is transferable to other envi-
580 ronments, spatio-temporal scales, and platforms. While it is likely a particular quirk of
581 the Beaufort Lens that filtering for reflection alone can produce a horizontal effective speed
582 that compensates for ray refraction and reflection, it is trivial to filter along other ways, like
583 number of turning points, to create a more diverse and informed set of multipath timefronts.
584 Though the majority of re-navigation results are within single-meter accuracy, future work
585 can examine how constellations of more LBL beacons can extend the operational domain
586 without adding an undesirable amount of error. One possibility is that, during a mission,

587 ICNN-like LBL implementations use a comparison of the GNSS self-position and acoustic po-
588 sitioning to invert for the ocean volume, linking how vertical and horizontal sound speed
589 structure impact transmission integrity. A fast tomographic estimate ([Deffenbaugh, 1997](#);
590 [Elisseeff *et al.*, 2002](#)), along with its uncertainty, can be continuously communicated to assets
591 underway to maintain contact or enable adaptive sampling. In this sense navigation and to-
592 mography converge on the same set of component technologies—position estimation, sound
593 speed parameterization estimation, ray path identification, and vehicle path optimization.

594 Spatio-temporal variability is a serious challenge for accurate real-time ranging. On
595 one hand, the effectiveness of eigenray filtering algorithm is likely only challenged by the
596 valid operational scales of a range independent propagation environment. Longer range
597 experiments may provide more time for eigenray filtering. A bootstrapping approach that
598 filters eigenrays for several randomly generated internal wave spectrums may compensate
599 for otherwise unknowable spatio-temporal variability. The model-aided component to the
600 eigenray filtering is compatible with vertical slices from any physically driven ocean model.
601 But in the long run, more accurate and higher resolution global circulation models are
602 needed to properly resolve features that alter ducted propagation at the scales discernible
603 to an acoustic modem. Through-the-sensor methods can resolve local features but would
604 require a degree of information sharing not readily supported on the acoustic channel for
605 large scale variability. But addressing the spatial and temporal scales of what can be solved
606 deterministically and what must be solved stochastically imposes a resolution constraint
607 that is at odds with computational overhead for real-time operations. Resolving features
608 inaccurately, or with a false sense of confidence, could be more harmful than contextualizing

609 the limitations of a range independent propagation over realistic bathymetry. Given that
610 AUV operations are often on smaller spatial and temporal scales, the added benefit of a
611 gridded model is quite small, and for features like the Beaufort Lens, not well resolved.

612 The methods presented in this paper, including the software projects ([Benjamin *et al.*, 2010](#);
613 [Schneider *et al.*, 2015](#); [Schneider and Schmidt, 2010](#)), are open source and platform
614 agnostic. Large AUVs, often large enough to support long duration and/or deep sea mis-
615 sions, would benefit from including diurnal or tidal effects for ranging. Gliders, though
616 generally low power and memory, have been equipped with acoustic modems. Their in-
617 ability to maintain position within a region of reliable acoustic path makes the impact of
618 an environmentally adaptive pseudorange estimation disproportionately positive. The ex-
619 act adjustments to the ensemble eigenray filtering are predicated on the expected sound
620 speed conditions and acoustic arrival structure; the problem is ripe application for other
621 simulation testbeds or machine learning methods. The continued development of embed-
622 ded acoustic processing on heterogenous platforms is fundamental to support a universal
623 underwater navigation scheme comparable to GNSS.

624 **ACKNOWLEDGMENTS**

625 We acknowledge the significant operational effort spearheaded by the LAMSS ICEX20
 626 team and all our collaborators. Bhatt was funded by a National Defense, Science, and
 627 Engineering Graduate Fellowship. This work was supported by the Office of Naval Research
 628 322-OA under ICEX20 (N00014-17-1-2474) and Task Force Ocean (N00014-19-1-2716).

629

630 Ballard, M. S., Badiey, M., Sagers, J. D., Colosi, J. A., Turgut, A., Pecknold, S., Lin,
 631 Y.-T., Proshutinsky, A., Krishfield, R., Worcester, P. F., and Dzieciuch, M. A. (**2020**).

632 “Temporal and spatial dependence of a yearlong record of sound propagation from the
 633 Canada Basin to the Chukchi Shelf,” The Journal of the Acoustical Society of America
 634 **148**(3), 1663–1680, doi: [10.1121/10.0001970](https://doi.org/10.1121/10.0001970).

635 Barker, L. D., Jakuba, M. V., Bowen, A. D., German, C. R., Maksym, T., Mayer, L.,
 636 Boetius, A., Dutrieux, P., and Whitcomb, L. L. (**2020**). “Scientific challenges and present
 637 capabilities in underwater robotic vehicle design and navigation for oceanographic explo-
 638 ration under-ice,” Remote Sensing **12**(16), 1–31, doi: [10.3390/RS12162588](https://doi.org/10.3390/RS12162588).

639 Bellingham, J. G., Leonard, J. J., Vaganay, J., Goudey, C. A., Atwood, D. K., Consi,
 640 T. R., Bales, J. W., Schmidt, H., and Chrysostomidis, C. (**1995**). “AUV operations in
 641 the Arctic,” in *Sea Ice Mechanics and Arctic Modeling Workshop*.

642 Benjamin, M. R., Schmidt, H., Newman, P. M., and Leonard, J. J. (**2010**). “Nested au-
 643 tonomy for unmanned marine vehicles with MOOS-IvP,” Journal of Field Robotics **27**(6),

- 644 834–875, doi: [10.1002/rob.20370](https://doi.org/10.1002/rob.20370).
- 645 Bhatt, E. C. (2021). “A Virtual Ocean framework for environmentally adaptive, embed-
646 ded acoustic navigation on autonomous underwater vehicles,” Ph.D. thesis, Woods Hole
647 Oceanographic Institution, doi: [10.1575/1912/27309](https://doi.org/10.1575/1912/27309).
- 648 Bhatt, E. C., Howard, B., and Schmidt, H. (2022). “An Embedded Tactical Decision Aid
649 Framework for Environmentally Adaptive Autonomous Underwater Vehicle and Commu-
650 nication,” IEEE Journal of Oceanic Engineering (accepted).
- 651 Brooke, J. (1981). “ARCS (Autonomous remotely controlled submersible),” in *Proceedings*
652 *of the 1981 2nd International Symposium on Unmanned Untethered Submersible Technol-*
653 *ogy*, IEEE, Vol. 2, p. 28.
- 654 Chassignet, E. P., Hurlburt, H. E., Smedstad, O. M., Halliwell, G. R., Hogan, P. J.,
655 Wallcraft, A. J., Baraille, R., and Bleck, R. (2007). “The HYCOM HYbrid Coordinate
656 Ocean Model data assimilative system,” Journal of Marine Systems **65**(1), 60–83, doi:
657 [10.1016/j.jmarsys.2005.09.016](https://doi.org/10.1016/j.jmarsys.2005.09.016).
- 658 Chen, R., Poulsen, A., and Schmidt, H. (2019). “Spectral, spatial, and temporal character-
659 istics of underwater ambient noise in the Beaufort Sea in 1994 and 2016,” The Journal of
660 the Acoustical Society of America **145**(2), 605–614, doi: [10.1121/1.5088601](https://doi.org/10.1121/1.5088601).
- 661 Chen, R., and Schmidt, H. (2020). “Temporal and spatial characteristics of the Beaufort
662 Sea ambient noise environment,” The Journal of the Acoustical Society of America **148**(6),
663 3928–3941, doi: [10.1121/10.0002955](https://doi.org/10.1121/10.0002955).
- 664 Claus, B., Kepper, J. H., Suman, S., and Kinsey, J. C. (2018). “Closed-loop one-way-travel-
665 time navigation using low-grade odometry for autonomous underwater vehicles,” Journal

- 666 of Field Robotics **35**(4), 421–434, doi: [10.1002/rob.21746](https://doi.org/10.1002/rob.21746).
- 667 Deffenbaugh, M. (1997). “Optimal Ocean Acoustic Tomography and Navigation with Mov-
- 668 ing Sources,” Phd thesis.
- 669 Deffenbaugh, M., Bellingham, J. G., and Schmidt, H. (1996a). “The relationship between
- 670 spherical and hyperbolic positioning,” in *OCEANS 96 MTS/IEEE Conference Proceedings*.
- 671 *The Coastal Ocean - Prospects for the 21st Century*, Vol. 2, pp. 590–595, doi: [10.1109/OCEANS.1996.568293](https://doi.org/10.1109/OCEANS.1996.568293).
- 672 Deffenbaugh, M., Schmidt, H., and Bellingham, J. G. (1996b). “Acoustic positioning in a
- 673 fading multipath environment,” in *OCEANS 96 MTS/IEEE Conference Proceedings*, Vol.
- 674 2, pp. 596—600, doi: [10.1109/OCEANS.1996.568294](https://doi.org/10.1109/OCEANS.1996.568294).
- 675 Duda, T. F., Morozov, A. K., Howe, B. M., Brown, M. G., Speer, K., Lazarevich, P.,
- 676 Worcester, P. F., and Cornuelle, B. D. (2006). “Evaluation of a Long-Range Joint Acoustic
- 677 Navigation Thermometry System,” in *OCEANS 2006*, pp. 1–6, doi: [10.1109/OCEANS.2006.306999](https://doi.org/10.1109/OCEANS.2006.306999).
- 678 Duda, T. F., Zhang, W. G., and Lin, Y.-T. (2021). “Effects of Pacific Summer Water layer
- 679 variations and ice cover on Beaufort Sea underwater sound ducting,” *J. Acoust. Soc. Am.*
- 680 21.
- 681 Duda, T. F., Zhang, W. G., Lin, Y.-T., and Newhall, A. E. (2019). “Long-range sound
- 682 propagation in the Canada Basin,” .
- 683 Elisseeff, P., Schmidt, H., and Xu, W. (2002). “Ocean acoustic tomography as a data
- 684 assimilation problem,” *IEEE Journal of Oceanic Engineering* **27**(2), 275–282, doi: [10.1109/JOE.2002.1002482](https://doi.org/10.1109/JOE.2002.1002482).

- 688 Eustice, R. M., Whitcomb, L. L., Singh, H., and Grand, M. (2006). “Recent advances in
689 synchronous-clock one-way-travel-time acoustic navigation,” in *Oceans 2006*, IEEE, pp.
690 1–6, doi: [10.1109/OCEANS.2006.306931](https://doi.org/10.1109/OCEANS.2006.306931).
- 691 Eustice, R. M., Whitcomb, L. L., Singh, H., and Grund, M. (2007). “Experimental Re-
692 sults in Synchronous-Clock One-Way-Travel-Time Acoustic Navigation for Autonomous
693 Underwater Vehicles,” in *Proceedings 2007 IEEE International Conference on Robotics*
694 and Automation, pp. 4257–4264, doi: [10.1109/ROBOT.2007.364134](https://doi.org/10.1109/ROBOT.2007.364134).
- 695 Fossum, T. O., Norgren, P., Fer, I., Nilsen, F., Koenig, Z. C., and Ludvigsen, M. (2021).
696 “Adaptive Sampling of Surface Fronts in the Arctic Using an Autonomous Underwater
697 Vehicle,” *IEEE Journal of Oceanic Engineering* **46**(4), 1155–1164, doi: [10.1109/JOE.2021.3070912](https://doi.org/10.1109/JOE.2021.3070912).
- 698
- 699 Freitag, L., Ball, K., Partan, J., Koski, P., and Singh, S. (2016). “Long range acoustic com-
700 munications and navigation in the Arctic,” in *OCEANS 2015 - MTS/IEEE Washington*,
701 IEEE, pp. 1–5, doi: [10.23919/oceans.2015.7401956](https://doi.org/10.23919/oceans.2015.7401956).
- 702 Graupe, C. E., Van Uffelen, L. J., Webster, S. E., Worcester, P. F., and Dzieciuch, M. A.
703 (2019). “Preliminary results for glider localization in the Beaufort Duct using broadband
704 acoustic sources at long range,” in *OCEANS 2019 MTS/IEEE Seattle, OCEANS 2019*,
705 IEEE, pp. 1–6, doi: [10.23919/OCEANS40490.2019.8962637](https://doi.org/10.23919/OCEANS40490.2019.8962637).
- 706 Gwal, A., and Jain, A. (2011). “GPS scintillation studies in the arctic region during the
707 first winter-phase 2008 Indian Arctic Expedition,” *Polar Science* **4**(4), 574–587, doi: [10.1016/j.polar.2010.08.001](https://doi.org/10.1016/j.polar.2010.08.001).
- 708

- 709 Hayes, D. R., and Morison, J. H. (2002). “Determining turbulent vertical velocity, and
710 fluxes of heat and salt with an autonomous underwater vehicle,” *Journal of Atmospheric
711 and Oceanic Technology* **19**(5), 759–779.
- 712 Howe, B. M., Miksis-Olds, J., Rehm, E., Sagen, H., Worcester, P. F., and Haralabus, G.
713 (2019). “Observing the Oceans Acoustically,” *Frontiers in Marine Science* **6**(JUL), 1–22,
714 doi: [10.3389/fmars.2019.00426](https://doi.org/10.3389/fmars.2019.00426).
- 715 Jackson, E. (1983). “Autonomous remotely controlled submersible ”ARCS”,” in *Proceedings
716 of the 1983 3rd International Symposium on Unmanned Untethered Submersible Technol-
717 ogy*, IEEE, Vol. 3, pp. 77–88.
- 718 Jakuba, M. V., Roman, C. N., Singh, H., Murphy, C., Kunz, C., Willis, C., Sato, T.,
719 and Sohn, R. A. (2008). “Long-baseline acoustic navigation for under-ice autonomous
720 underwater vehicle operations,” *Journal of Field Robotics* **25**(11-12), 861–879, doi: <https://doi.org/10.1002/rob.20250>.
- 721
- 722 Jung, T. S., Hegel, T. M., Bentzen, T. W., Egli, K., Jessup, L., Kienzler, M., Kuba, K.,
723 Kukka, P. M., Russell, K., Suitor, M. P., and Tatsumi, K. (2018). “Accuracy and per-
724 formance of low-feature GPS collars deployed on bison *Bison bison* and caribou *Rangifer
725 tarandus*,” *Wildlife Biology* **2018**(1), doi: [10.2981/wlb.00404](https://doi.org/10.2981/wlb.00404).
- 726 Kepper, J. H., Claus, B. C., and Kinsey, J. C. (2017). “MEMS IMU and one-way-travel-
727 time navigation for autonomous underwater vehicles,” in *OCEANS 2017 - Aberdeen*, IEEE,
728 Aberdeen, UK, pp. 1–9, doi: [10.1109/OCEANSE.2017.8084842](https://doi.org/10.1109/OCEANSE.2017.8084842).
- 729 Krishfield, R., Toole, J., Proshutinsky, A., and Timmermans, M. L. (2008). “Automated
730 ice-tethered profilers for seawater observations under pack ice in all seasons,” *Journal of*

- 731 Atmospheric and Oceanic Technology **25**(11), 2091–2105, doi: [10.1175/2008JTECH0587](https://doi.org/10.1175/2008JTECH0587).
- 732 1.
- 733 Kukulya, A., Plueddemann, A., Austin, T., Stokey, R., Purcell, M., Allen, B., Littlefield, R.,
- 734 Freitag, L., Koski, P., Gallimore, E., Kemp, J., Newhall, K., and Pietro, J. (2010). “Under-
- 735 ice operations with a REMUS-100 AUV in the Arctic,” in *2010 IEEE/OES Autonomous*
- 736 *Underwater Vehicles, AUV 2010*, IEEE, pp. 1–8, doi: [10.1109/AUV.2010.5779661](https://doi.org/10.1109/AUV.2010.5779661).
- 737 Kunz, C., Murphy, C., Camilli, R., Singh, H., Bailey, J., Eustice, R., Jakuba, M., Nakamura, K. I., Roman, C., Sato, T., Sohn, R. A., and Willis, C. (2008). “Deep sea underwater
- 738 robotic exploration in the ice-covered arctic ocean with AUVs,” in *2008 IEEE/RSJ Interna-*
- 739 *tional Conference on Intelligent Robots and Systems, IROS*, IEEE, pp. 3654–3660, doi:
- 740 [10.1109/IROS.2008.4651097](https://doi.org/10.1109/IROS.2008.4651097).
- 741 Light, R. D., and Morison, J. (1989). “The Autonomous Conductivity-Temperture Vehicle:
- 742 First in the Seashuttle Family of Autonomous Underwater Vehicle’s for Scientific Pay-
- 743 loads,” in *Proceedings OCEANS*, Vol. 3, pp. 793–798, doi: [10.1109/OCEANS.1989.586683](https://doi.org/10.1109/OCEANS.1989.586683).
- 744 Litvak, A. G. (2015). “Acoustics of the deepwater part of the Arctic Ocean and of Russia’s
- 745 Arctic shelf,” *Herald of the Russian Academy of Sciences* **85**(3), 239–250, doi: [10.1134/S1019331615030144](https://doi.org/10.1134/S1019331615030144).
- 746 Mikhalevsky, P. N., Sperry, B. J., Woolfe, K. F., Dzieciuch, M. A., and Worcester, P. F.
- 747 (2020). “Deep ocean long range underwater navigation,” *The Journal of the Acoustical*
- 748 *Society of America* **147**(4), 2365–2382, doi: [10.1121/10.0001081](https://doi.org/10.1121/10.0001081).
- 749 National Research Council (2011). *National Security Implications of Climate Change for*
- 750 *U.S. Naval Forces* (National Academies Press, Washington, D.C.).

- 753 Norgren, P., Lubbad, R., and Skjetne, R. (2014). “Unmanned underwater vehicles in Arctic
754 operations,” in *Proceedings of the 22nd IAHR International Symposium on Ice. Singapore,*
755 pp. 89–101.
- 756 Paull, L., Saeedi, S., Seto, M., and Li, H. (2014). *AUV Navigation and Localization: A*
757 *Review*, **39**, pp. 131–149.
- 758 Plueddemann, A. J., Kukulya, A. L., Stokey, R., and Freitag, L. (2012). “Autonomous
759 Underwater Vehicle Operations Beneath Coastal Sea Ice,” IEEE/ASME Transactions on
760 Mechatronics **17**(1), 54–64, doi: [10.1109/TMECH.2011.2174798](https://doi.org/10.1109/TMECH.2011.2174798).
- 761 Porter, M. B. (2011). “The bellhop manual and user’s guide: Preliminary draft,” .
- 762 Poulsen, A. J., and Schmidt, H. (2017). “Acoustic noise properties in the rapidly changing
763 Arctic Ocean,” Proceedings of Meetings on Acoustics (28), 1–10, doi: [10.1121/2.0000552](https://doi.org/10.1121/2.0000552).
- 764 Randeni, S., Schneider, T., and Schmidt, H. (2020). “Construction of a high-resolution
765 under-ice AUV navigation framework using a multidisciplinary virtual environment,” in
766 *2020 IEEE/OES Autonomous Underwater Vehicles Symposium, AUV 2020*, IEEE, pp.
767 1–7, doi: [10.1109/AUV50043.2020.9267950](https://doi.org/10.1109/AUV50043.2020.9267950).
- 768 Randeni, S., Schneider, T., Schmidt, H., Bhatt, E., and Viquez, O. (2021). “A high-
769 resolution AUV navigation framework with integrated communication and tracking for
770 under-ice deployments,” Field Robotics (in review).
- 771 Reid, T., Walter, T., Blanch, J., and Enge, P. (2016). “GNSS Integrity in The Arctic,”
772 *Navigation* **63**(4), 469–492, doi: [10.1002/navi.169](https://doi.org/10.1002/navi.169).
- 773 Rossby, T., Dorson, D., and Fontaine, J. (1986). “The RAFOS System,” *Journal of*
774 *Atmospheric and Oceanic Technology* **3**(4), 672–679, doi: [10.1175/1520-0426\(1986\)003;4-672.TRAFOS.1](https://doi.org/10.1175/1520-0426(1986)003;4-672.TRAFOS.1)

775 003<0672:TRS>2.0.CO;2.

776 Rypkema, N. R., Fischell, E. M., and Schmidt, H. (2017). “One-Way Travel-Time Inverted

777 Ultra-Short Baseline Localization for Low-Cost Autonomous Underwater Vehicles,” in *2017*

778 *IEEE International Conference on Robotics and Automation*, Singapore, pp. 4920–4926.

779 Schmidt, H., and Schneider, T. (2016). “Acoustic communication and navigation in the

780 new Arctic — A model case for environmental adaptation,” 2016 IEEE Third Underwa-

781 ter Communications and Networking Conference (UComms) 1–4, doi: [10.1109/UComms.2016.7583469](https://doi.org/10.1109/UComms.2016.7583469).

782 Schneider, T., Petillo, S., Schmidt, H., and Murphy, C. (2015). “The dynamic compact

783 control language version 3,” in *OCEANS 2015-Genova*, IEEE, pp. 1–7.

784 Schneider, T., and Schmidt, H. (2010). “Unified command and control for heterogeneous

785 marine sensing networks,” *Journal of Field Robotics* **27**(6), 876–889, doi: <https://doi.org/10.1002/rob.20346>.

786 Schneider, T., and Schmidt, H. (2018). “NETSIM: A Realtime Virtual Ocean Hardware-in-

787 the-loop Acoustic Modem Network Simulator,” in *2018 Fourth Underwater Communica-*

788 *tions and Networking Conference (UComms)*, IEEE, pp. 1–5, doi: [10.1109/UComms.2018.8493188](https://doi.org/10.1109/UComms.2018.8493188).

789 Schneider, T., Schmidt, H., and Randeni, S. (2021). “Self-Adapting Under-Ice Integrated

790 Communications and Navigation Network,” 2021 Fifth Underwater Communications and

791 Networking Conference (UComms) 1–5, doi: [10.1109/UComms50339.2021.9598012](https://doi.org/10.1109/UComms50339.2021.9598012).

792 Singh, S., Grand, M., Bingham, B., Eustice, R., Singh, H., and Freitag, L. (2006). “Un-

793 derwater acoustic navigation with the WHOI Micro-Modem,” in *Oceans 2006*, IEEE, pp.

- 797 1–4, doi: [10.1109/OCEANS.2006.306853](https://doi.org/10.1109/OCEANS.2006.306853).
- 798 Swanlund, D., Maraj, R., Schuurman, N., Hope, R., Donkers, K., Aquin, M., and Rickerby,
- 799 G. (2016). “Gps performance in yukon’s arctic coast,” Geografiska Annaler: Series A,
- 800 Physical Geography **98**(4), 361–368, doi: [10.1111/geoa.12143](https://doi.org/10.1111/geoa.12143).
- 801 Themens, D. R., Jayachandran, P. T., and Langley, R. B. (2015). “The nature of GPS
- 802 differential receiver bias variability: An examination in the polar cap region,” Journal of
- 803 Geophysical Research: Space Physics **120**(9), 8155–8175, doi: [10.1002/2015JA021639](https://doi.org/10.1002/2015JA021639).
- 804 Timmermans, M.-L., and Winsor, P. (2013). “Scales of horizontal density structure in the
- 805 Chukchi Sea surface layer,” Continental Shelf Research **52**, 39–45.
- 806 Toole, J., Krishfield, R., Timmermans, M.-L., and Proshutinsky, A. (2011). “The Ice-
- 807 Tethered Profiler: Argo of the Arctic,” Oceanography **24**(3), 126–135, doi: [10.5670/oceanog.2011.64](https://doi.org/10.5670/oceanog.2011.64).
- 808
- 809 Van Uffelen, L. J., Howe, B. M., Nosal, E. M., Carter, G. S., Worcester, P. F., and Dzieci-
- 810 uch, M. A. (2016). “Localization and subsurface position error estimation of gliders using
- 811 broadband acoustic signals at long range,” IEEE Journal of Oceanic Engineering **41**(3),
- 812 501–508, doi: [10.1109/JOE.2015.2479016](https://doi.org/10.1109/JOE.2015.2479016).
- 813 Van Uffelen, L. J., Nosal, E.-M., Howe, B. M., Carter, G. S., Worcester, P. F., Dzieciuch,
- 814 M. A., Heaney, K. D., Campbell, R. L., and Cross, P. S. (2013). “Estimating uncertainty
- 815 in subsurface glider position using transmissions from fixed acoustic tomography sources,”
- 816 The Journal of the Acoustical Society of America **134**(4), 3260–3271, doi: [10.1121/1.4818841](https://doi.org/10.1121/1.4818841).
- 817

- 818 Van Uffelen, L. J. V. (2021). “Global Positioning Systems: Over Land and Under Sea,”
819 Acoustics Today **17**(1), 9.
- 820 Webster, S. E., Eustice, R. M., Singh, H., and Whitcomb, L. L. (2009). “Preliminary
821 deep water results in single-beacon one-way-travel-time acoustic navigation for underwater
822 vehicles,” in *2009 IEEE/RSJ International Conference on Intelligent Robots and Systems,*
823 *IROS 2009*, IEEE, pp. 2053–2060, doi: [10.1109/IROS.2009.5354457](https://doi.org/10.1109/IROS.2009.5354457).
- 824 Webster, S. E., Eustice, R. M., Singh, H., and Whitcomb, L. L. (2012). “Advances in single-
825 beacon one-way-travel-time acoustic navigation for underwater vehicles,” *The International
826 Journal of Robotics Research* **31**(8), 935–950, doi: [10.1177/0278364912446166](https://doi.org/10.1177/0278364912446166).
- 827 Webster, S. E., Freitag, L. E., Lee, C. M., and Gobat, J. I. (2015). “Towards real-time
828 under-ice acoustic navigation at mesoscale ranges,” in *Proceedings - IEEE International
829 Conference on Robotics and Automation*, IEEE, Vol. 2015-June, pp. 537–544, doi: [10.
830 1109/ICRA.2015.7139231](https://doi.org/10.1109/ICRA.2015.7139231).
- 831 Wu, M., Barmin, M. P., Andrew, R. K., Weichman, P. B., White, A. W., Lavely, E. M.,
832 Dzieciuch, M. A., Mercer, J. A., Worcester, P. F., and Ritzwoller, M. H. (2019). “Deep
833 water acoustic range estimation based on an ocean general circulation model: Application
834 to PhilSea10 data,” *The Journal of the Acoustical Society of America* **146**(6), 4754–4773,
835 doi: [10.1121/1.5138606](https://doi.org/10.1121/1.5138606).